NAVAL POSTGRADUATE SCHOOL
Monterey, California

THESIS

AN EXPERIMENTAL STUDY OF A PIN-FIN HEAT EXCHANGER

by

David Ramthun

June 2003

Thesis Advisor: Ashok Gopinath

Approved for public release; distribution is unlimited

THIS PAGE INTENTIONALLY LEFT BLANK

REPORT DOCUMENTATION PAGE			Form Approved OMB No. 0704-0188
Public reporting burden for this collection of information is estimated to average 1 hour per response, including the time for reviewing instruction, searching existing data sources, gathering and maintaining the data needed, and completing and reviewing the collection of information. Send comments regarding this burden estimate or any other aspect of this collection of information, including suggestions for reducing this burden, to Washington headquarters Services, Directorate for Information Operations and Reports, 1215 Jefferson Davis Highway, Suite 1204, Arlington, VA 22202-4302, and to the Office of Management and Budget, Paperwork Reduction Project (0704-0188) Washington DC 20503.			
1. AGENCY USE ONLY *(Leave blank)*	**2. REPORT DATE** June 2003	**3. REPORT TYPE AND DATES COVERED** Master's Thesis	
4. TITLE AND SUBTITLE: An Experimental Study of a Pin-Fin Heat Exchanger			**5. FUNDING NUMBERS**
6. AUTHOR(S) David Ramthun			
7. PERFORMING ORGANIZATION NAME(S) AND ADDRESS(ES) Naval Postgraduate School Monterey, CA 93943-5000			**8. PERFORMING ORGANIZATION REPORT NUMBER**
9. SPONSORING /MONITORING AGENCY NAME(S) AND ADDRESS(ES) Naval Air Systems Command Patuxent River, MD			**10. SPONSORING/MONITORING AGENCY REPORT NUMBER**
11. SUPPLEMENTARY NOTES The views expressed in this thesis are those of the author and do not reflect the official policy or position of the Department of Defense or the U.S. Government.			
12a. DISTRIBUTION / AVAILABILITY STATEMENT Approved for public release; distribution is unlimited			**12b. DISTRIBUTION CODE**

13. ABSTRACT ***(maximum 200 words)***

A detailed experimental study has been carried out on the heat transfer and pressure drop characteristics of a compact heat exchanger with pin fins. A modular wind-tunnel with a rectangular cross-section duct-flow area was constructed that would accommodate the heat exchanger test section with varying pin designs. The flow in the tunnel was achieved through a suction-type blower, and a leading entrance length section was added to achieve predictable flow conditions into the heat exchanger test section. The rig was comprehensively instrumented to provide all desired thermal and flow data. The results from this study provide useful empirical data to validate ongoing numerical studies of such heat exchanger designs.

14. SUBJECT TERMS compact heat exchanger, experimental study, pin-fin array			**15. NUMBER OF PAGES** 79
			16. PRICE CODE
17. SECURITY CLASSIFICATION OF REPORT Unclassified	**18. SECURITY CLASSIFICATION OF THIS PAGE** Unclassified	**19. SECURITY CLASSIFICATION OF ABSTRACT** Unclassified	**20. LIMITATION OF ABSTRACT** UL

NSN 7540-01-280-5500 Standard Form 298 (Rev. 2-89)
Prescribed by ANSI Std. 239-18

THIS PAGE INTENTIONALLY LEFT BLANK

Approved for public release; distribution is unlimited

AN EXPERIMENTAL STUDY OF A PIN FIN HEAT EXCHANGER

David L. Ramthun
Lieutenant, United States Navy
B.S.M.E., North Carolina State University, 1997

Submitted in partial fulfillment of the
requirements for the degree of

MASTER OF SCIENCE IN MECHANICAL ENGINEERING

from the

NAVAL POSTGRADUATE SCHOOL
June 2003

Author: David L. Ramthun

Approved by: Ashok Gopinath
Thesis Advisor

Young W. Kwon
Chairman, Department of Mechanical Engineering

THIS PAGE INTENTIONALLY LEFT BLANK

ABSTRACT

A detailed experimental study has been carried out on the heat transfer and pressure drop characteristics of a compact heat exchanger with pin fins. A modular wind-tunnel with a rectangular cross-section duct-flow area was constructed that would accommodate the heat exchanger test section with varying pin designs. The flow in the tunnel was achieved through a suction-type blower, and a leading entrance length section was added to achieve predictable flow conditions into the heat exchanger test section. The rig was comprehensively instrumented to provide all desired thermal and flow data. The results from this study provide useful empirical data to validate ongoing numerical studies of such heat exchanger designs.

THIS PAGE INTENTIONALLY LEFT BLANK

TABLE OF CONTENTS

LIST OF FIGURES

LIST OF TABLES

THIS PAGE INTENTIONALLY LEFT BLANK

ACKNOWLEDGMENTS

Kelly Ramthun, Spouse; for her understanding and patience

Dr. Ashok Gopinath, Thesis Advisor; for his guidance and knowledge

CDR Len Hamilton, PHD Student, PE; for his generosity, patience, and open door

Frank Franzen, NPS Model Maker; for his dedication and assistance

Jim Lefler, NPS Model Maker; for his attention to detail and persistence

Tom Christian, Lab Technician; for his generosity and patience

Shelia Deiotte, Lab Technician; for her commitment and tenacity

Marie Beals, Purchasing Agent; for her dedication and efficiency

NAVAIR, for funding and support

THIS PAGE INTENTIONALLY LEFT BLANK

I. INTRODUCTION

The motivation for this thesis primarily stems from a desire to improve the design and performance of large area density compact heat exchangers. They find use in various applications such as the cooling of turbine blades, which can dramatically extend the material service life of the blades and allow for higher operating temperatures. The cooling of circuit boards and computer chips can also use this type of cooling strategy for large heat flux removal rates.

There currently isn't a satisfactory model to accurately calculate the performance of short cross- pin heat exchangers with pins having a height to diameter ratio close to unity. In the absence of a model that can represent short cross pin heat exchangers, actual turbine blades typically are required to be built and tested. This can be extremely expensive and laborious. Additionally, there are structural design limits to consider [Chyu, 1999] when designing the turbine blades. The design of these cooling methods could be more easily iterated and improved if it could be simulated with a suitable numerical model. Previous and current work [Hamilton, 2003] has provided full three dimensional finite element models for various short cross pin heat exchangers using commercial finite element computer software to provide a numerical solution. Experimental data is needed to verify these numerical models. The numerical models have been compared to results from previous experimental studies [Hamilton, 2003], but a more inclusive comparison of varying pin configurations has been deemed necessary. An experimental test apparatus was built to accomplish this task. The construction, successful operation of the test apparatus with preliminary pin configurations and good correlations with the numerical models and other experimental results was the motivation for this thesis.

THIS PAGE INTENTIONALLY LEFT BLANK

II. BACKGROUND AND OBJECTIVES

A. BACKGROUND THEORY

It is common practice to verify numerical computer model solutions with experimental data. It is not, however, practical to simulate all possible characteristics with a numerical model; some variables in the computer model must be speculated on as discretionary. These conjectures may cause the numerical method to be inaccurate. The validity of the numerical solution is also a function of the turbulence model used by the computational fluid dynamic (CFD) software. The shortfalls of the CFD turbulence model usually occur in the modeling of the turbulence paths in the re-circulating region behind the pins [Shah, 2001]. Additionally, as with any finite element model, the numerical model is limited in accuracy by mesh density.

B. PREVIOUS WORK

1. Metzger

Metzger [1982] established some of the early results for short cross-pin heat exchangers. His work has been used as the baseline for comparisons for other experimental results. He conducted experimental testing on short cross pin heat exchanger configurations. Metzger's contributions lead to the analysis of the row-by-row analysis of a staggered pin heat exchanger array. He concluded that for all Reynolds numbers there is an initial rise in the row averaged Nusselt number over the first three to five rows after which it remains fairly constant. He also determined that the peak heat transfer coefficient occurred earlier in the array with the longer X/D ratio (2.5) than the array with the smaller X/D ratio (1.5). Metzger additionally states that the average heat transfer is higher for arrays with smaller X/D.

2. Arora

Arora [1989] conducted an experimental study similar to that of Metzger in that he conducted a row-by-row analysis of a compact heat exchanger. Arora's contributions state that the averaged array friction factor increased as the blockage increased due to different arrangement of the pin fin geometries. Additionally, Arora studied the thermal and flow effects of oblong pin fins. He determined that they do not offer any advantage over round pins unless used with the short profile parallel to the airflow.

3. Chyu

Chyu [1989] studied the effects of heat and mass transfer on compact heat exchangers using the technique of naphthalene sublimation. The erosion of the naphthalene was then correlated to the heat transfer at various points on the staggered pin array. Chyu studied the effects of the end walls and pins with fillets on the heat transfer coefficient. He concluded that the existence of these fillets produced lower heat transfer coefficients and higher-pressure drops. Therefore, the fillets were determined to be undesirable.

4. Current Experimental Setup

The current experimental test apparatus was intended to simulate an isothermal condition at the end plates and an insulated condition at the side plates. By using a highly conductive material, the pins were also intended to simulate an isothermal condition. To establish row-by-row data, the alternating five pin and four pin rows were thermally insulated. These boundary conditions were set to allow an accurate comparison to the numerical model.

One key objective of this experimental setup was to allow for simple alterations in the pin sizes and shapes. The aforementioned experiments used different end plates with the pins being attached with an epoxy or using an interference fit. In this experiment, the pins attached to the end plates with screws, thus the pins could be easily changed. This attachment technique was tested for accuracy through the electrical resistance analogy and found to be acceptable.

All the previous experiments covered different aspects of the various arrays. This experimental setup was intended to completely cover the pressure drop, row-by-row heat transfer, and friction factor characteristics of several staggered cross-pin heat exchanger configurations. For a minimal cost the heat exchanger test array could be altered to provide a test platform for numerous cross-pin designs.

C. CURRENT OBJECTIVES

The objectives of this thesis were to design, build and successfully operate a modular pin fin heat exchanger test apparatus. The design parameters required it to be capable of simple alterations, therefore providing numerous configuration possibilities to

allow experimental data to be collected over a large range of flow rates and temperatures. Once design and construction were complete, the test apparatus was to be calibrated and compared with published experimental results. Then tests of various pin shapes, sizes and configurations were to be conducted. With each new pin configuration, the flow rates and temperatures were to be varied and compared to their respective numerical model solutions and other experimental results. Once the test apparatus was successfully compared to other experimental results, it was to be used to provide validity to numerical models currently being researched. The final goal was to develop a robust experimental apparatus capable of supporting future pin fin heat exchanger designs in support of the ongoing research program on micro-heat exchangers.

THIS PAGE INTENTIONALLY LEFT BLANK

III. EXPERIMENTAL SETUP

A. MODEL CONFIGURATION: INTERATIONS AND SIZING

The driving factor in the initial dimensions of the model grew from the calculated pressure drop across the heat exchanger section. The blower needed to be capable of providing the required flow rates, at the associated pressure drops, as calculated by the numerical solution and from a simple estimate using Bernoulli's equation (1), conservation of mass and volumetric flow rate. As the selection of a blower proceeded, the availability and capabilities of affordable and reliable blowers determined the amount of pressure drop across and flow through the test apparatus. After taking into consideration the Reynolds numbers that were to be tested, the associated mass flow rates, the pressure drop of the system, and the price, as well as the reliability, led to the purchase of the blower as listed in the parts list. All of the previous iterations were compared to the numerical solution results for a consensus.

$$\frac{P_{in}}{\rho}+\frac{V_{in}^2}{2}+Z_{in}g=\frac{P_{out}}{\rho}+\frac{V_{out}^2}{2}+Z_{out}g \qquad (1)$$

After the blower was chosen, the mass flow rate and pressure drop capabilities of the blower drove the scale of the heat exchanger section. The scaling matched closely with commercially available flexible heaters. The heater's power capacity was chosen based on the maximum heat transfer from the corresponding numerical solution. The heaters had to be custom ordered with holes to maintain the flexible design theme of the heat exchanger section.

The purpose of the entrance section was to insure a fully developed, turbulent velocity profile entering the heat transfer section. Knowing the maximum Reynolds number the apparatus was estimated to be capable of providing, the required entrance length for that Reynolds number was calculated and increased for margin of error as well as ease of manufacture.

The mass-flow meter was chosen for its accuracy and capabilities, as published by the manufacturer, based on the blower parameters and the data from the numerical models. The voltage supply and output of the corresponding mass flow meter transmitter

were compatible with the voltages available and the data collection techniques that were to be implemented.

The test section exit duct was designed to re-direct the flow from the rectangular cross-section of the heat exchanger section to the circular cross-section of the mass flow meter piping. It was constructed from heavy gage steel plate to ensure it would not collapse under negative pressures. The ends were designed with material thick enough to handle the compression necessary to obtain an airtight seal using rubber gasket material. It was hypothesized that the flow characteristics of the air transition from rectangular to circular would also provide good mixing for exit temperature measurements, assuming minimal heat loses.

The mass flow meter installation procedure called for a length of inlet and exit pipe to ensure adequate flow straightening as recommended by the manufacturer. In order to alleviate any problems from that aspect, the inlet and outlet pipe sections were made according to the worse case scenario, alleviating the need for additional flow straightening.

The remainder of the apparatus was assembled to accommodate the blower inlet and the pipe diameter of the mass flow meter. One design aspect was using the blower to draw air through the test apparatus rather than forcing it into the inlet. This technique removed the need for bulk temperature calculations of the inlet air temperature into the heat exchanger section, as the blower would increase the air temperature. By keeping the inlet air temperature to a minimum, the heater ambient loses would be lower due to lower operating temperatures. The flow rates were varied by bypassing the test section downstream of the mass flow meter and by lowering the flow rate through the inlet with filters. This method of flow control permitted flexibility, durability and low cost, as well as ease of repeatability.

B. MODEL DESIGN AND MANUFACTURE

1. Overview

The components for the apparatus were drawn with commercially available CAD software to allow for easier communication during the manufacturing process. This

made changes easier to complete in a timely manner. As with any prototype, there were changes that were implemented to minister to ease of manufacture, assembly and fit.

One design aspect for the thermal separation of the rows was to allow for a row-by-row analysis and comparison. By having the row data, a more detailed comparison to the numerical model could be conducted as well as comparison to the results from Metzger [1982] and Aurora [1985]. The row sections also allowed for a closer simulation of an isothermal surface by the plates, as the adjacent rows would not be affected.

2. Inlet Sections

The inlet sections (Figure 1) were made of commercially available, half-inch thick Plexi-glass. This material was chosen to reduce the friction losses. They were designed so that there would be minimal flow interruptions and allow for ease of handling and manufacture. Additionally, they were designed to be flexible in their short side height. Their dimensions were analogous to the inside dimensions of the heat exchanger. For future testing configurations, different side plates may be constructed with minimal manufacturing time, to provide fully developed turbulent air for different heat exchanger designs. This would allow for varying test section height (H) dimensions. The minimum entrance length to achieve a fully developed turbulent velocity profile for a Reynolds Number of 100,000 would be about 2.4 meters, based on the cross section of the inlet sections as calculated by equation (2). The three inlet sections were constructed in 3 ft lengths to allow enough entrance length for a full range of Reynolds numbers. The sections were assembled using rubber gasket material as listed in the parts list. For more detailed drawings see appendix A.

$$L_e = 4.4\,\mathrm{Re}_d^{1/6}\, d_h \quad \text{where:}$$
$$d_h = \frac{4A}{\wp} \qquad A = WH \qquad \wp = 2\left(W + H\right) \tag{2}$$

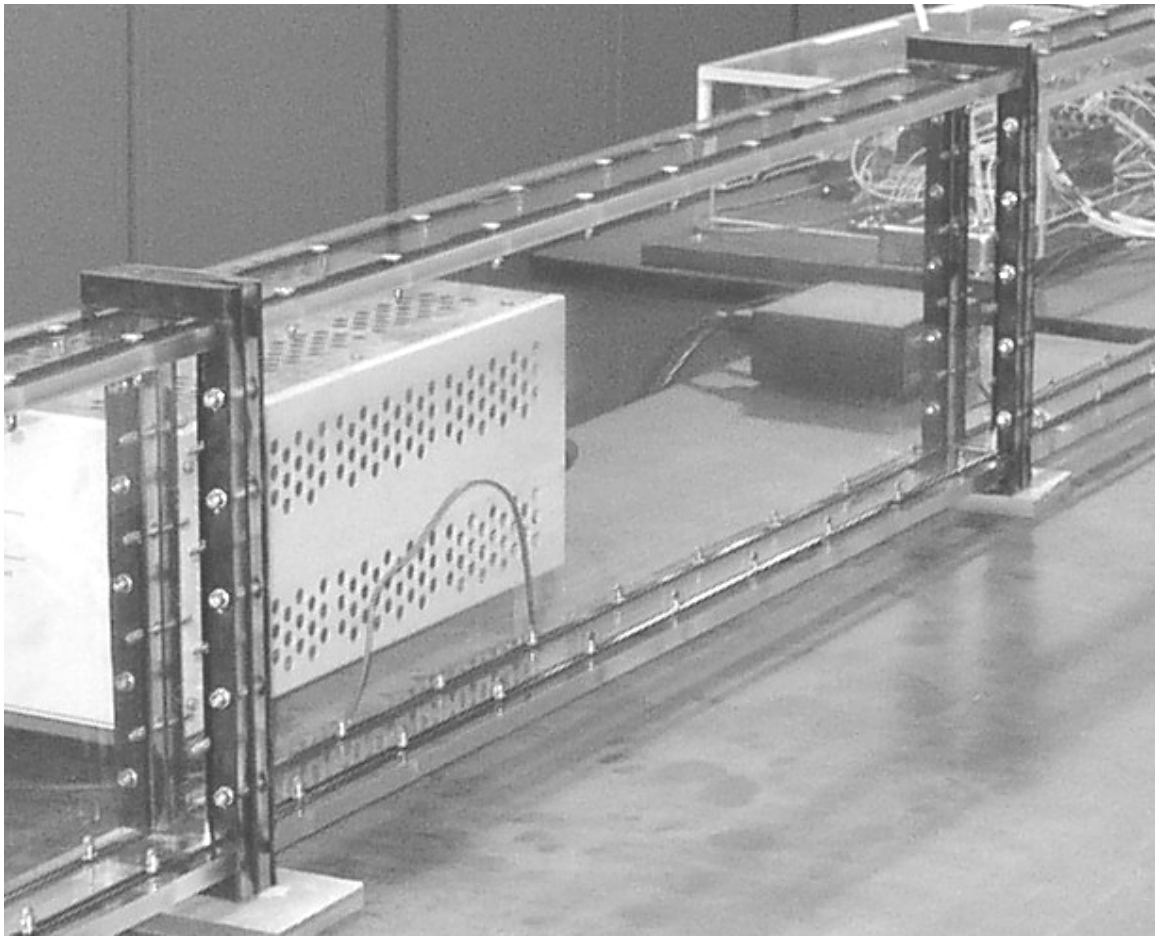

Figure 1. Inlet duct section

3. Cross Pin Heater Test Section

The test section (Figure 2) was constructed from 6061 T6 aluminum plate and rod. Aluminum was chosen because of its good conduction properties, ease of machining, resistance to corrosion/tarnishing and minimal cost. The sides of the test section were made from half inch Plexi-glass. The use of Plexi-glass minimized the amount of heat transfer through the sides, had a smooth surface to decrease the flow losses due to friction, and was easy to machine. It also allowed for easy inspection as shown in Figure 2.

The aluminum plate was machined into 250 x 50mm x 1/2-inch sections. A 1/16th inch o-ring groove was machined into the plate sections to provide for the addition of an o-ring for an airtight seal once assembled (Figure 2). To ensure minimal heat conduction between the sections and to allow for row-by-row observations and heater control, 1/32nd

inch Lexan spacers were manufactured and inserted between the plates during assembly. $1/8^{th}$ inch dowels were used between the plates to keep alignment of the sections and to prevent the spacers from moving during assembly and impeding the flow during operation. The dowels were made of wood to prevent the conduction of heat between sections (Figure 3). The completed test section has Plexi-glass end spacers (Figure 4) which prevent conduction of heat from the plates to the ducting and to hold the test section together. Additionally, the spacers provided surface area for bolting the test section to the rest of the ducting and a smooth surface for the gasket material.

The various pin shapes and sizes were constructed from the previously mentioned aluminum rod. They were sized to provide various dimensional ratios (S/D, X/D, H/D) to simulate the numerical models. They were attached to the end plates with stainless steel machine screws through holes in the plates. The assembly and pin dimensions can be viewed in the drawings in appendix C.

There was concern about surface contact between the pins and the plates. The design of tapped holes in the pins and recessed screws through the top plates was tested using electrical resistances checks on a sample pin with plate model. This test revealed little electrical resistance, even without removing the protective coating on the aluminum plate surface. This low electrical resistance, and the analogy to conduction resistance [Weills, 1949], eliminated the concern, as the apparatus was to be used to measure data only in steady state conditions. Once the test section was completely assembled, the electrical checks were repeated with successful results.

Slots were machined into the outside of each plate from the closest hole then to the center Figure 3. The thermocouples were routed through the holes in the heaters, along the slots, to the midsection of the four pin sections and between the center pin and next closest on the five-pin sections Figure 5. The thermocouple positions were established from a thermal mapping process that was conducted on preliminary test sections in conjunction with heater control system testing. The mapping established that position was irrelevant provided that the thermocouple was anywhere near the center of the plate sections.

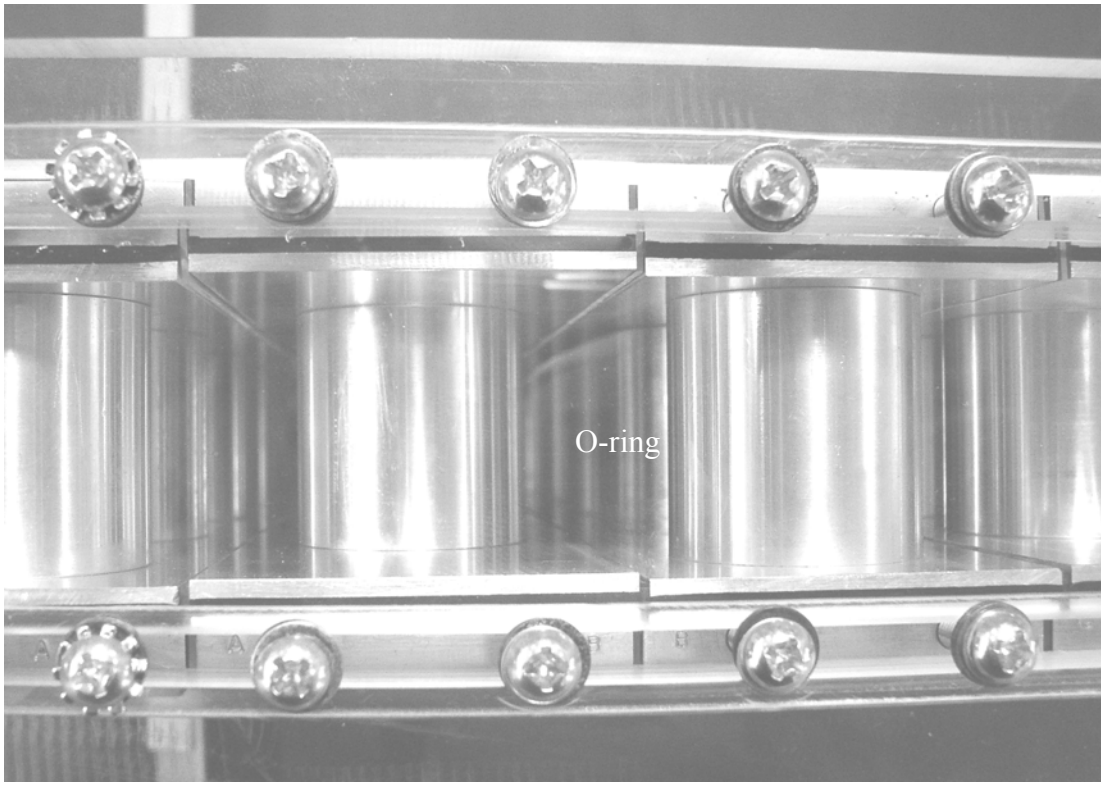

Figure 2. Test section side view close up

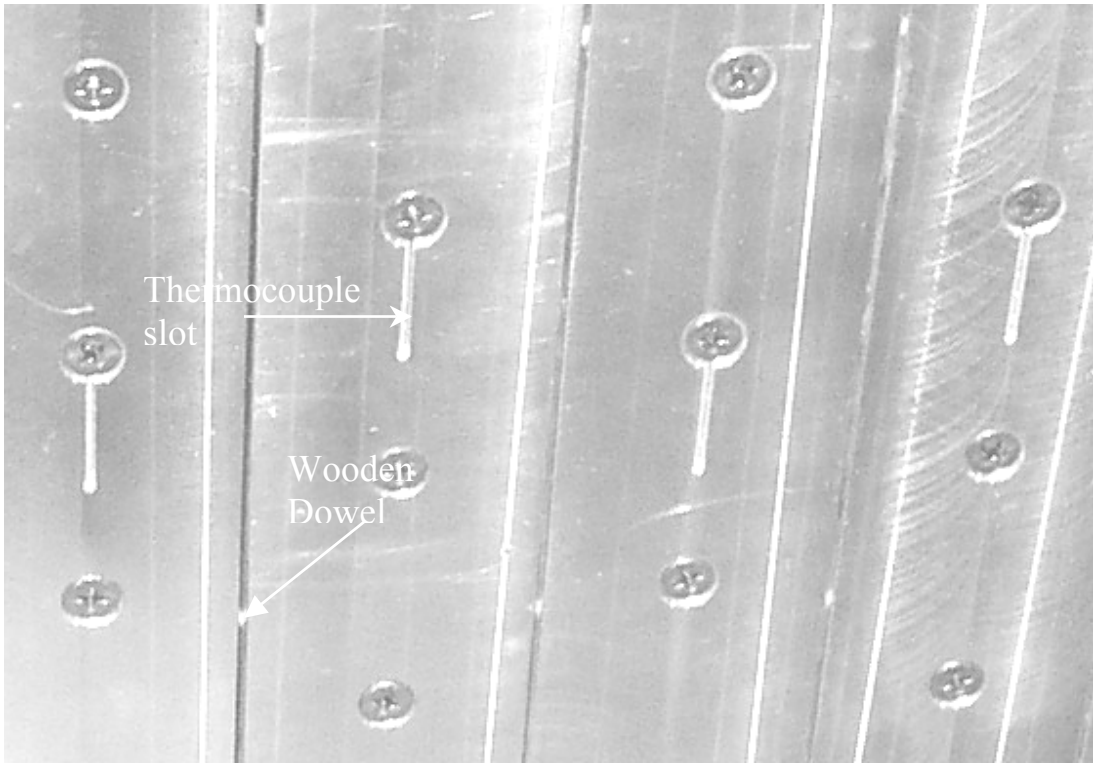

Figure 3. Thermocouple slots in top plates and Lexan spacers

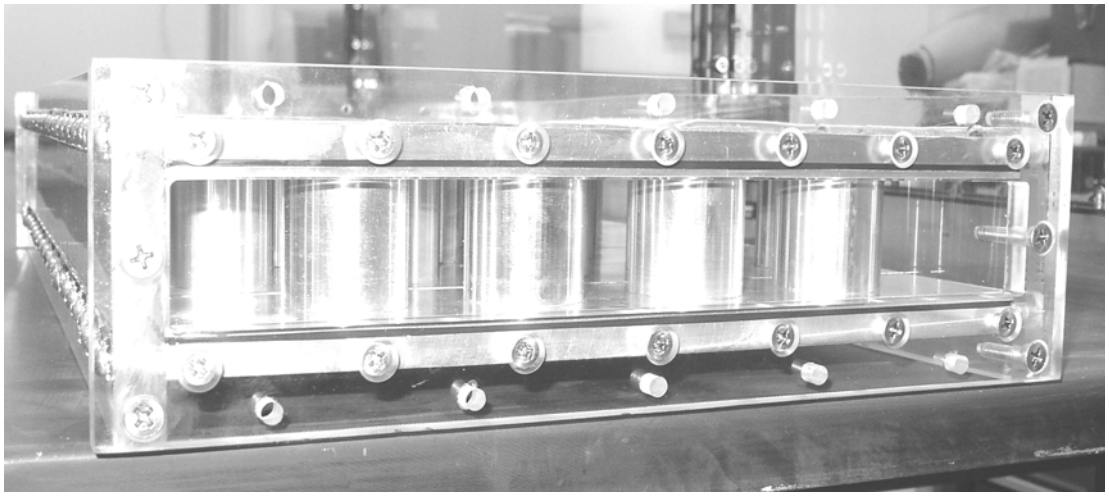

Figure 4. End spacer for heater test section

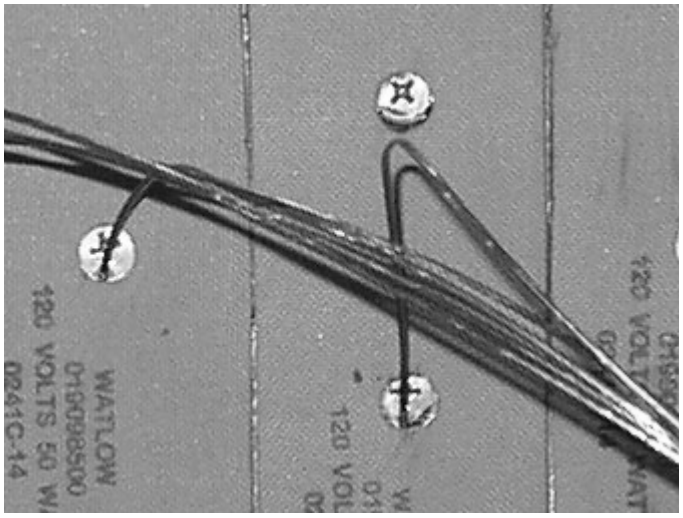

Figure 5. Thermocouple wire routing

4. Heaters

The heaters were ordered with 10 mm holes, precut by the manufacturer as requested (Figure 6). The outer dimensions and the spacing of the holes corresponded with the size and bolt pattern of the plates on the heat exchanger test sections. The holes in the heaters allow for thermocouple wire access and the ability to change the pins (rotate the pin mounting screws) in the heat exchanger section without removing the heaters. The heater power rating of 50 Watts per heater was based on the numerical model solution results of a maximum of 1000 Watts total at the highest Reynolds number the experimental setup should achieve (~50,000). The heaters were adhered with thermally conductive epoxy listed in the parts list in appendix D.

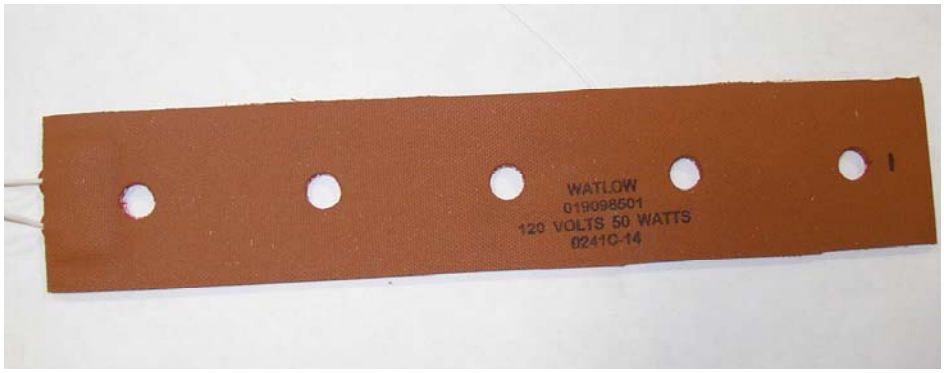

Figure 6. Five hole Watlow heater

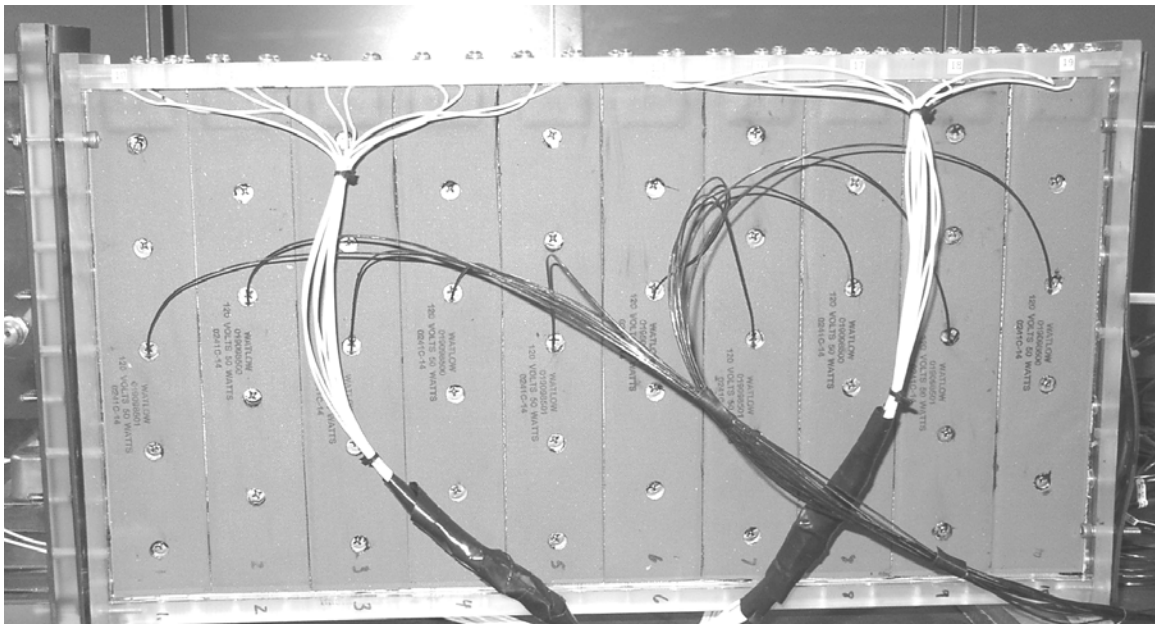

Figure 7. Test section heaters

5. Exit Duct

El Camino Machine, in Salinas, California, provided the CAD drawing in Figure 8 and manufactured the exit duct as per dimensions of the end cross sections. The square end matched the bolt pattern of the end spacer and the round end aligned with the bolt holes of the 2 ½-inch PVC flange leading to the flow straightening section. The outlet pressure tap was mounted in this duct. The duct was insulated with 1½-inch rigid foam insulation, cut to fit, to reduce the thermal losses, in an attempt to measure the bulk temperature at the flange between this duct and the flow straightening section Figure 9.

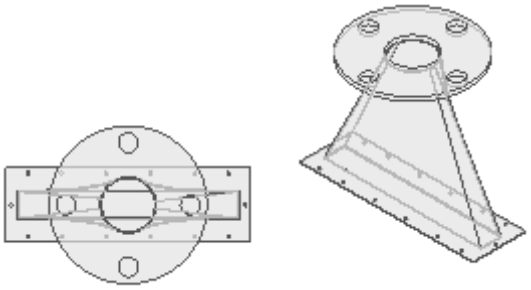

Figure 8. CAD drawing of exit duct section

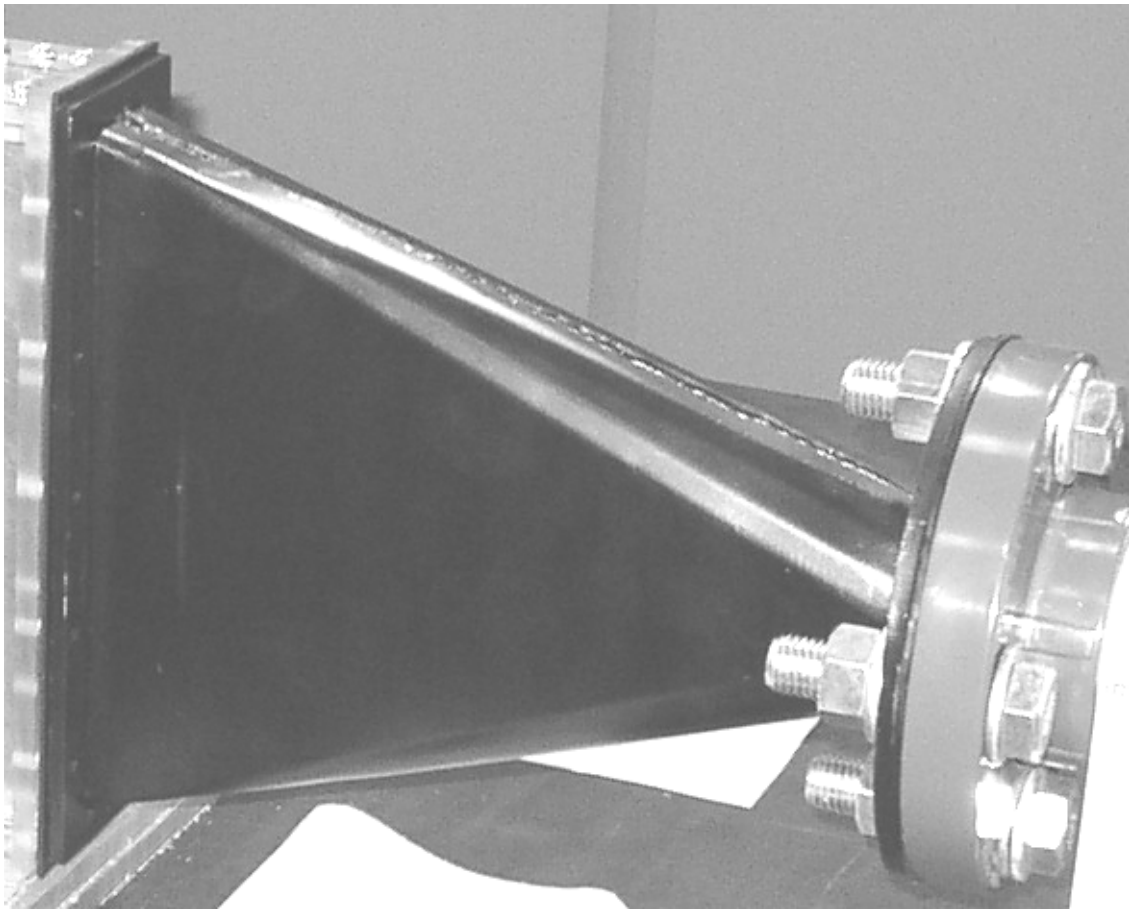

Figure 9. Exit duct

6. Mass Flow Meter and Piping

The mass flow meter was chosen based on its capabilities. It is capable of accurately registering low and high flow ranges, which meets the testing criteria. It is also compatible with the data collection system. The flanges threaded onto the mass flow meter were 2 ½ inch standard steel flanges. There were minor gaps in the connections, subjecting the flow to turbulence from exposed threads and ridges. Cutting and gluing

rubber sheeting, to provide as smooth a transition as possible, filled the gaps Figure 10. Additionally, the PVC flanges on the flow straightening sections were machined to remove the ridge that exists to stop the PVC pipe from extending past the flange Figure 11.

Figure 10. Treaded flanges for mass flow meter

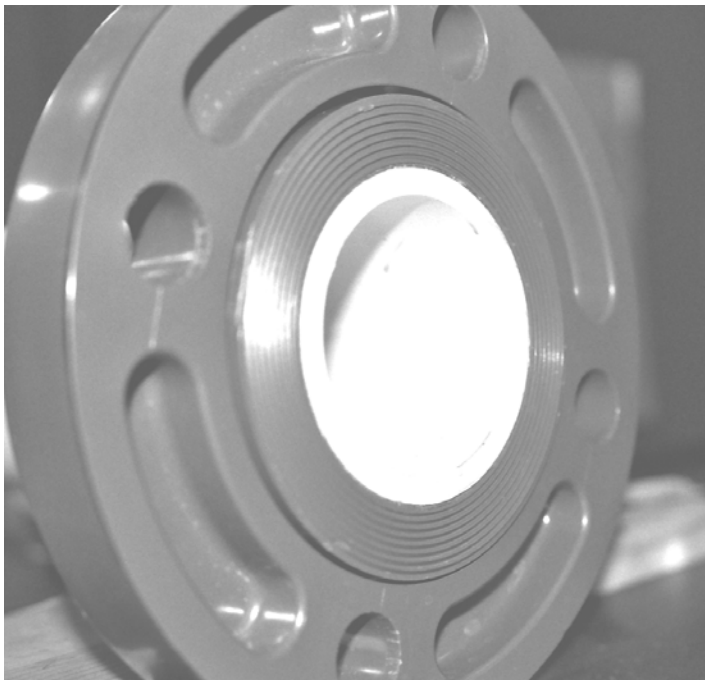

Figure 11. Bolted flanges for mass flow meter

7. Valves and Blower

The bypass valves were installed to alleviate the need for variable blower motor control. Globe valves were chosen because of their capability to throttle flow more effectively than gate or butterfly type valves. Because of the restrictive nature of globe valves, however, two valves were installed in parallel to ensure adequate bypass flow rates. Opening and/or closing the bypass valves vary the flow rates without the blower operating outside of characteristics. As the test apparatus was operated, it was determined that there was not enough bypass capability. To provide lower flow rates an additional bypass technique was employed. Another PVC tee was added to the system and a threaded cap was used to open and close that bypass route.

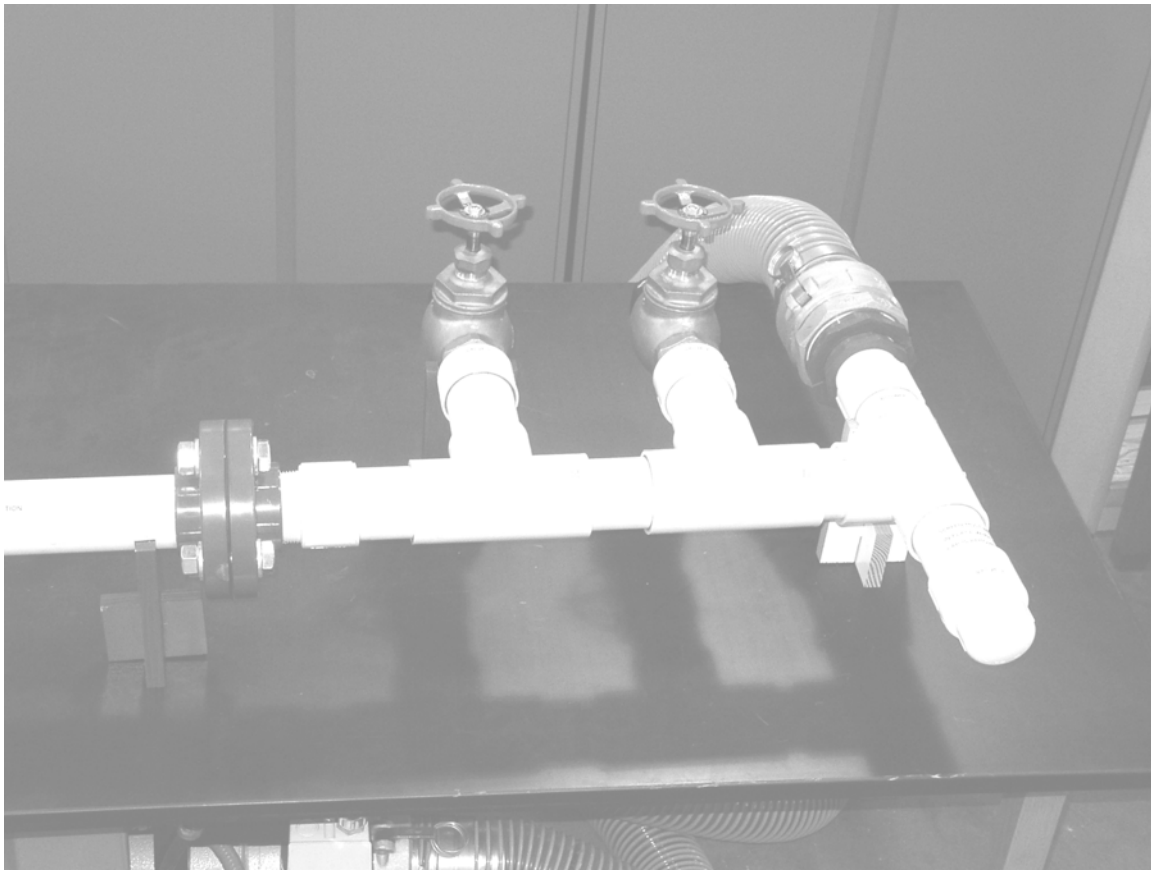

Figure 12. Bypass system and blower attachment

The blower was mounted on a mobile base to add portability. Vibration isolation dampers were mounted between the blower and the base in an attempt to lower the possibility of the motion of the blower base during operation overcoming the caster brakes. The blower connected to the test apparatus by means of flexible ducting and

quick-disconnect fittings. The power to the blower was by means of an electrical cord permanently wired to the blower and capable of inserting into a standard outlet.

8. Apparatus Assembly

The parts to the test apparatus were cleaned, inspected, and assembled using good engineering practices. The pieces for the test section were carefully assembled, ensuring good fit and surface contact for an airtight seal. After passing the thermal couple wires through the appropriate heater holes, the thermal couples were held in their slots on the test section by compressing the edges of the machined slots with a punch. This allowed the test section to be handled while applying the conductive epoxy. Once the epoxy used on the thermal couples cured, the heaters were attached using the same conductive epoxy.

The assembly of the remainder of the test apparatus was completed and checked for air leaks. To ensure that a good surface contact was occurring between the pins and the plates, a resistance check was conducted between the screws holding the top plates to the side plates and those screws holding the pins to the top plates. Also, resistance checks between the sections showed that good insulation between the sections was occurring. Once the air leak and resistance checks were satisfactory, the apparatus was wired and preliminary testing on the case I (see section V) pins was conducted.

IV. EXPERIMENTAL TESTING

A. FLOW CALIBRATION

1. Flow Meter and Transmitter

The manufacturer provided calibration data with the flow meter and transmitter (Tables 1 and 2). The calibration data was plotted using Microsoft Excel and the linear fit trend line function was used to find the equation of the trend line. This is displayed on Figure 13 and Figure 14.

Knowing the equation of the respective trend lines, an association or conversion factor was calculated.

Table 1. Manufacturer calibration data for flow meter

Calibration Data			Conversions	
Pulses/sec	K [pulses/acf]	Q [acf/sec]	Q [acf/min]	Q[m^3/s]
1027.4236	131.52994	7.811328736	468.6797242	0.221192198
917.7682	131.53099	6.977581481	418.6548889	0.197583104
812.3649	132.46224	6.132803582	367.9682149	0.173661658
695.9073	131.84075	5.278393061	316.7035837	0.149467447
592.1823	132.14931	4.481160742	268.8696445	0.126892341
480.793	132.77132	3.621211268	217.2726761	0.102541284
374.4457	132.45919	2.826875961	169.6125576	0.080048213
268.4616	132.45945	2.026745544	121.6047326	0.057391043
159.7085	131.52611	1.214272208	72.85633248	0.03438436
46.8041	131.20926	0.356713391	21.40280343	0.010100998

Table 2. Manufacturer calibration data for flow meter transmitter

Calibration Data	
Input Frequency	Output Voltage [VDC]
0	0
237.5	2.532
475	5.03
712.5	7.53
950	10

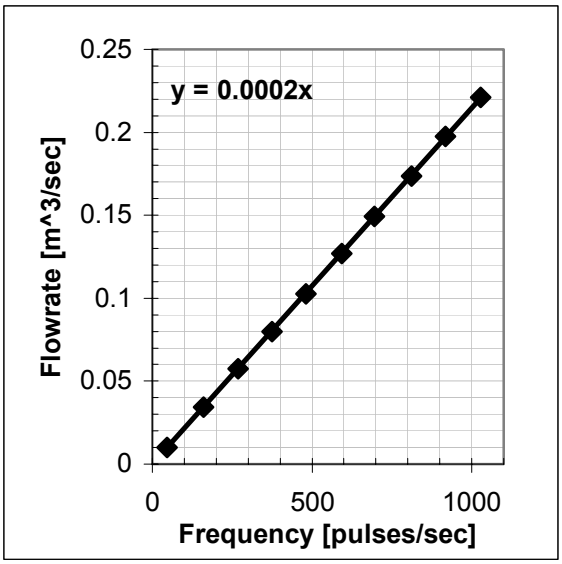

Figure 13. Linear fit to flow meter calibration data

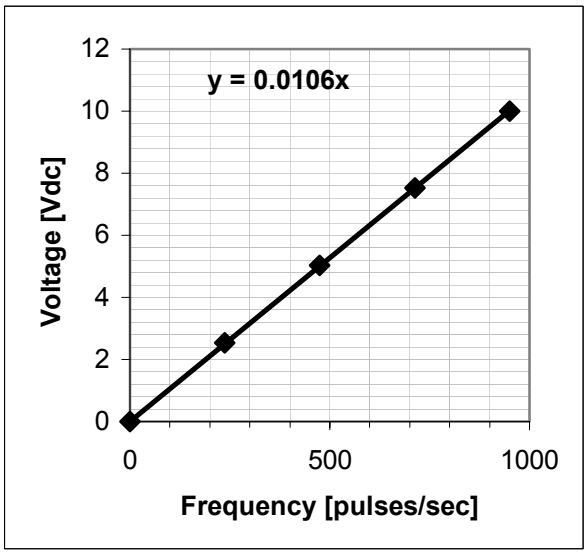

Figure 14. Linear fit to transmitter calibration data

2. Flow Meter Transmitter Bench Test

The flow meter transmitter was tested to alleviate any doubt as to the accuracy of the output voltage, given a specific frequency input. The calibration sheets from the manufacturer used a voltage supply of 15 VDC and in this application a voltage of 24 VDC was employed. The voltage supply to be used during operational use (24 VDC) was energized and a signal generator used to provide the various input signals to simulate the flow meter turbine output. The voltage outputs at the transmitter, as well as the voltage measured by the data collection system and displayed on the computer, were

recorded, as seen in Table 3. The measured data is shown graphically on Figure 15. The results of the Excel trend line fit function to the measured data were sufficiently similar to the results from the manufacturer's data, lending to the application of the manufacturers calibration data for the conversion from volts to volumetric flow rate.

Table 3. Flow meter transmitter bench test data

300 mV PP Sine input		
Frequency [Hz]	Meter [Vdc]	computer [Vdc]
50	0.551	0.552
100	1.073	1.074
150	1.594	1.594
200	2.116	2.115
250	2.637	2.635
300	3.158	3.158
350	3.68	3.677
400	4.2	4.198
450	4.722	4.719
500	5.241	5.239
550	5.76	5.76
600	6.282	6.281
650	6.801	6.799
700	7.322	7.32
750	7.842	7.838
800	8.361	8.359
850	8.881	8.877
900	9.398	9.396
950	9.916	9.916
200 mV Sine input		
950	9.917	9.917
100 mV Sine input		
950	9.92	9.918

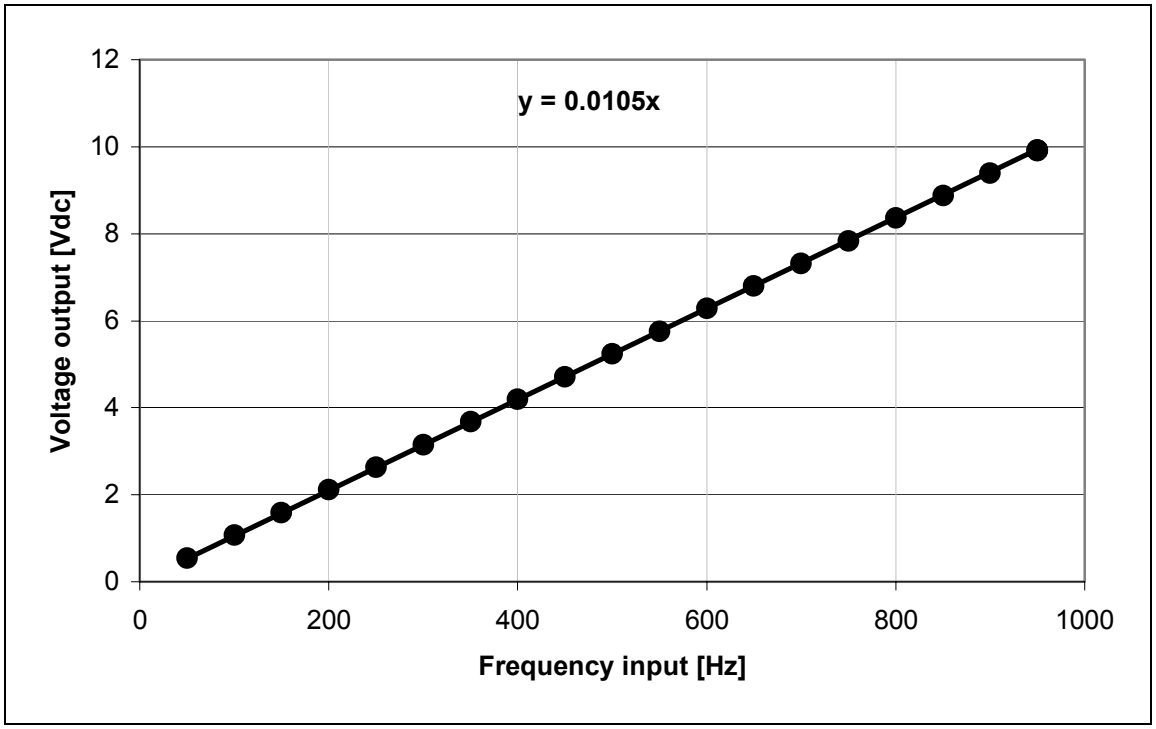

Figure 15. Linear fit to bench test calibration

B. PRESSURE TRANSDUCER CALIBRATION

The differential pressure transducer calibration sheet from the manufacturer shows that it was calibrated with a voltage supply of 24 VDC. In an attempt to avoiding the need for calibration (not recommended as per the manufacturer), the voltage provided to the pressure transducer from the test apparatus remained at 24 VDC. Due to the level of uncertainty (0.25% of FS voltage), the transducer was compared at different flow conditions to a horizontally mounted inclined manometer. The comparison showed that the pressure transducer read within the advertised accuracy at various differential pressures. The calibration data was plotted, the units converted and curve fit using Excel (Figure 16).

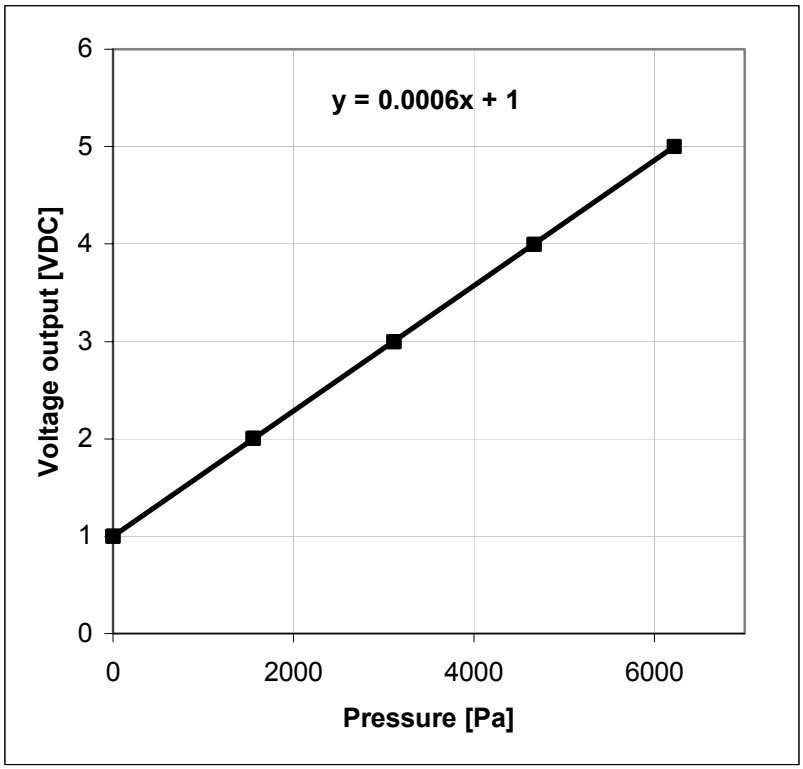

Figure 16. Plot of calibration data for differential pressure transducer

C. HEATER CONTROL AND DATA AQUISITION

1. Heater Control

The heaters were controlled using National Instruments, LABVIEW software. Tom Christian and Shelia Deiotte wrote, edited, and tested, this control system code as necessary to achieve heater system control and data collection. They sought and ordered the necessary components to interface the computer with the heaters and guided the assembly of the HP3852A data acquisition unit, as well as the wiring of the heater relays, system thermal couples, mass flow meter, and pressure transducer.

Setting the desired temperature on the LABVIEW software operated the heaters. The software read the thermal couple temperature via the HP3852A and associated computer interface card. As the software scanned the thermal couples, it send an on or off signal to the heater relays via the HP3852A. This maintained the surface of the aluminum plates at the desired temperature. There were three control systems designed in the LABVIEW software, an on/off controller, a slope controller, and a PID type controller. The first was chosen for its simplicity and adequate functionality.

2. Data Acquisition Process

The LABVIEW software monitored the associated channel number, temperatures or voltages, and on or off signal (one for on, zero for off) from the HP3852A. This data and the time stamp from the computer were recorded in a 'tab delimited' column format that could be opened with Microsoft Excel. The software also displayed real time data in the form of an operating window. This operating window provided a visual display that allowed the operator to see the state of the heaters (on or off), the time stamp, the mass flow rate and pressure transducer voltages, and four of forty selectable thermal couple readings, as well as controlling the desired temperature setting for the heaters. Additionally, the software had control of whether and where the data was being recorded and if the HP3852A was scanning or in standby. A pictorial reproduction of the control screen and the system diagram can be seen in Figure 17.

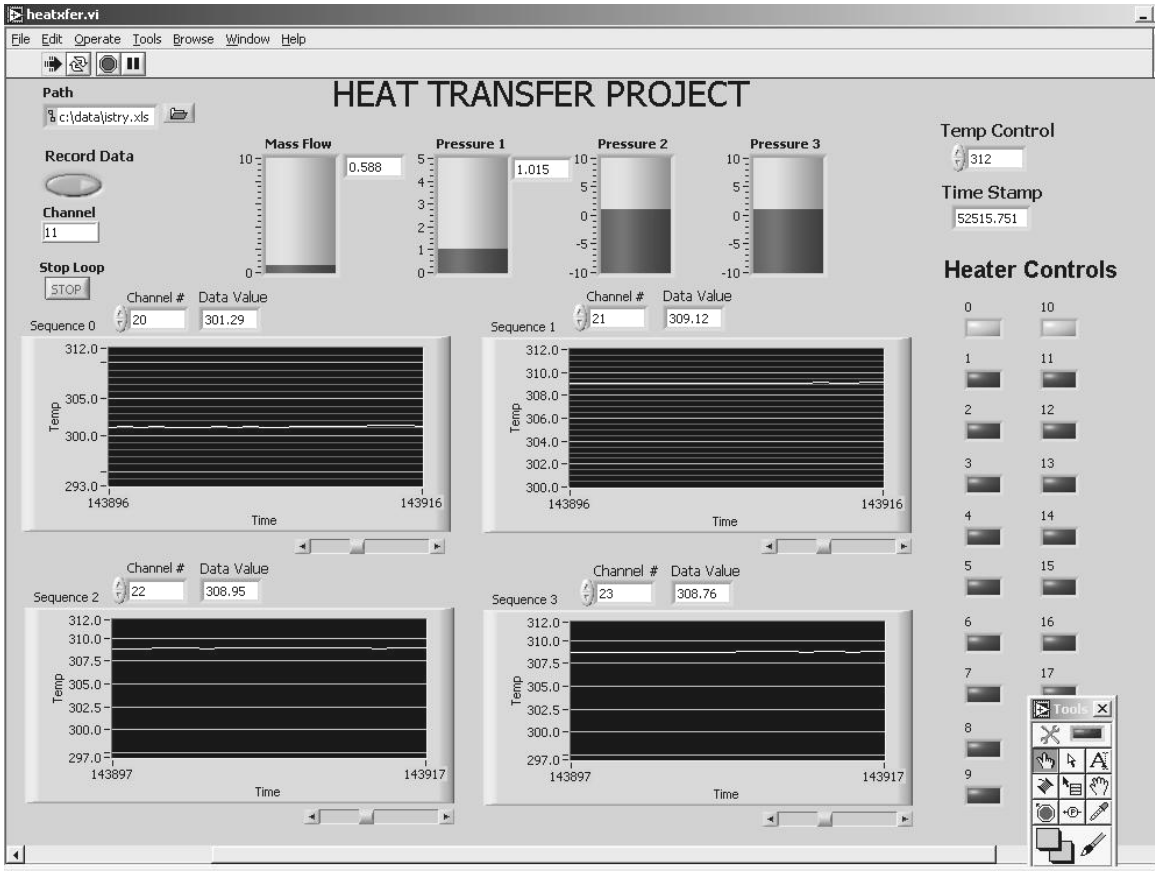

Figure 17. LABVIEW control window

D. TESTING PROCEDURE

1. Operation

It was determine that the electrical equipment required warming before consistent voltage readings were seen. This was particularly evident from the mass flow meter and pressure transducer output voltage fluctuations. Once the voltages were stable, they were recorded for future use as offset measurements to be subtracted from the recorded voltages during the test run calculations. These offsets were also checked at the completion of the days testing and typically proved to be the same values they were after initial stabilization.

The first step prior to conducting a series of tests for a particular ΔT above ambient was a 20 minute zero flow run to determine the ambient losses from the test section heaters at the current ambient conditions. This was initially repeated again at the end of the run to check for changes due to varying atmospheric conditions. It was found that there were minimal changes and the final zero flow run was regarded as unnecessary.

As the testing was conducted the atmospheric temperature was measured and recorded as initial inlet temperature by the data collection software via a thermal couple installed at the entrance to the inlet section of the test apparatus. The atmospheric pressure data was obtained from the National Oceanic and Atmospheric Administration (NOAA) website (www.wrh.noaa.gov) data as reported for the local airport, then recorded.

With the test apparatus sufficiently warmed, the zero flow test complete and the data recorded, the blower was started. Once the blower was up to operating speed and the flow conditions to be tested were set, the pressure tube for the pressure transducer was removed and the voltage measuring the differential pressure at the entrance to the end duct section (downstream of heater test section) with respect to atmosphere was recorded. This pressure measurement was later used to calculate the density prior to entrance to the flow straightening section. This process was repeated according to the different configurations as in the following section. The data for each run was copied from the associated file, as recorded to by the LABVIEW software, to an appropriately labeled worksheet in Microsoft Excel format.

Once all the tests to be conducted for the test period were complete, the test apparatus was secured by covering all opening into the apparatus to keep foreign objects from effecting future operations. Additionally, all electrical power was secured to the equipment via predetermined methods, unplugging or on/off switch.

2. Data Calculations

With the data from each test run and the voltage measurements for the offsets of the mass flow meter and pressure transducer, as well as the NOAA atmospheric data, and requested temperature settings for the end plates, a MATLAB code written for this purpose was used to calculate and output the data necessary for comparison to other experimental results and the numerical model solution.

The MATLAB code used the XLSREAD function to input the raw data to a matrix. This matrix was then read, according to the channel numbers specific to the data needed, and converted to individual matrices. Once the data was separated, the calculations were accomplished (see sample calculations in appendix). Function files were used to calculate the row-by-row energy transferred (Q). One aspect of the row-by-row measurement of the electrical power data was that the resistance of the heaters varied with the number of holes. A measurement of the resistances showed a consistent value based on the number of holes in the heater. This knowledge was implemented in the MATLAB code during the row-by-row calculation of the energy transferred. With the heat transferred to each row known, then the Nusselt number and heat transfer coefficients could be calculated.

Knowing the power of each heater and the amount of time it was energized the amount of the energy transferred was calculated. The Brand Power meter was used to double-check this process. There were no differences detected.

V. RESULTS AND DISCUSSION

A. EXPERIMENTAL MATRIX

The test apparatus was operated over the parameter range of the test matrix listed in Table 4. The two different turbulence generators listed were installed in the union between inlet section and the heated test section to explore the role of incoming free stream turbulence. This technique of varying the different parameters gave twenty-eight test runs/points for each case for comparison to other experimental data and the numerical model solution.

Table 4. Test Matrix

	Configuration	Reynolds Number	Flow and temperature settings
Case I 33mm	H/D = 1	Seven numbers ranging: ~4500 to ~45000	$\Delta T = +6$
	S/D = 1.5		$\Delta T = +12$
	X/D = 1.5		$\Delta T = +12$ & Strip turbulence filter
			$\Delta T = +12$ & Screen turbulence filter
Case II 16.5mm	H/D = 2	Seven numbers ranging: ~4500 to ~45000	$\Delta T = +6$
	S/D = 3		$\Delta T = +12$
	X/D = 3		$\Delta T = +12$ & Strip turbulence filter
			$\Delta T = +12$ & Screen turbulence filter

The first pin configuration, case I, was based on a height versus diameter ratio (H/D) of one, a lateral spacing ratio (S/D) of 1.5 and a longitudinal spacing ratio (X/D) of 1.5. The measurement of these ratios is illustrated in Figure 18. The second pin configuration, case II, consisted of an S/D and X/D of 3 with a H/D of 2. This was accomplished by disassembly of the test section and replacing the 33 mm diameter cross pins used for case I with 16.5 mm diameter pins.

With the parameters and measured data of the experimental test known and the numerical model data for the same range of Reynolds numbers for the same pin configuration, a comparison of the Nusselt number, heat transfer coefficient, friction factor and pressure drop was achieved.

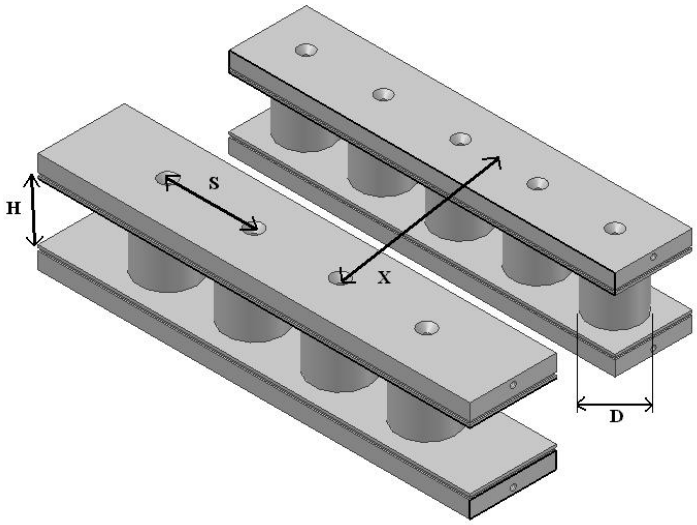

Figure 18. S, H, X and D portrayal

B. NUSSELT NUMBER RESULTS

1. Total Array Results

The Reynolds number was calculated from its definition as shown in the sample calculations in Appendix. For a number-to-number comparison, the results of the experimental data calculation of the Reynolds number required a numerical model to be run at the same Reynolds number. As this data was not available, the Reynolds number versus Nusselt number ratio for each experimental test point and pin configuration was graphed concurrently with the numerical data for comparison. There were seven different Reynolds numbers tested by varying the flow with different bypass valve configurations or by adding different flow obstructions to the entrance of the test apparatus as listed in Table 4. The Reynolds number ranged from about 4500 to 45000, providing a good range for comparison. This was done at a ΔT of 6 C above ambient. For a ΔT of 12 C above ambient three runs were done for the range of Reynolds numbers. One test was run without a turbulence generator and two test runs with different turbulence generators.

The Reynolds number was calculated from the recorded LABVIEW data with a MATLAB code. The MATLAB code was additionally used to calculate the heat transfer coefficient with the inlet temperature and the measured time each of the heaters were energized. With the calculated outlet temperature of the first row, it was used as the inlet temperature to the second row. This process was repeated for the entire array. This gave

an array outlet temperature. The heat transfer coefficient for the array was then calculated using the log-mean of the temperature. Knowing the heat transfer coefficient, the thermal conductivity of the air, and the hydraulic diameter, the Nusselt number was calculated.

The array Nusselt number comparison as a function of Reynolds number for the case I pins can be viewed in Figure 19. The comparison shows that there was an excellent correlation between the experimental and numerical results. Figure 20, which is based on the experimental results of a delta temperature of twelve degrees above ambient and the equivalent pin configuration numerical results, shows an even better correlation. A comparison of the "plus twelve" and "plus six" delta temperature runs for case I (Figure 21) shows little or no variation in the Nusselt number Reynolds number ratio based on the temperature difference above ambient. This assessment narrows the discussion to the plus twelve data, as this is the data with the turbulence generation.

These graphs of the comparison of the Nusselt number verses Reynolds number for case I (Figures 20 and 21) show the experimental results diverging slightly at the higher Reynolds numbers. It was conjectured that this could be due to a temperature gradient along the length of the pins. The temperature gradient was due to the greater heat transfer rate at the middle of the pin due to greater convection associated with the higher fluid velocity near the center of the heat exchanger test section. This is even more evident in the graphs of the case II results, Figures 22 and 23.

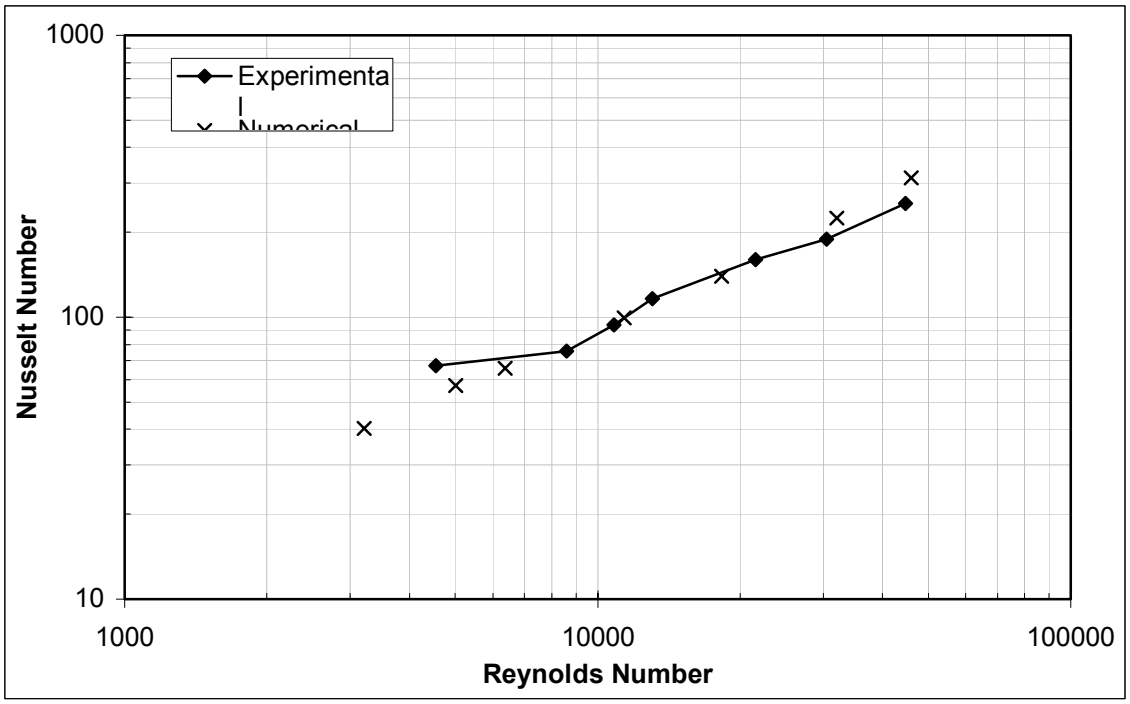

Figure 19. Results for Nusselt number for case I. Numerical data from Hamilton [2003] shown for comparison

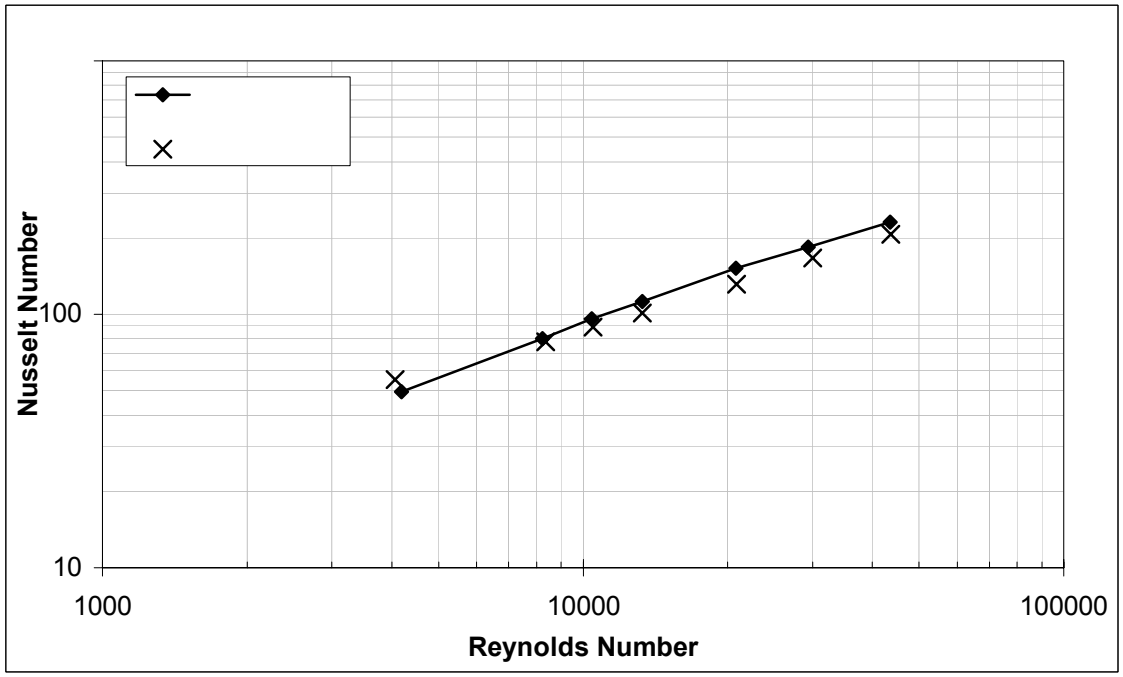

Figure 20. Nusselt Number vs. Reynolds Number for case I with gross turbulent generator. Numerical data from Hamilton [2003] shown for comparison

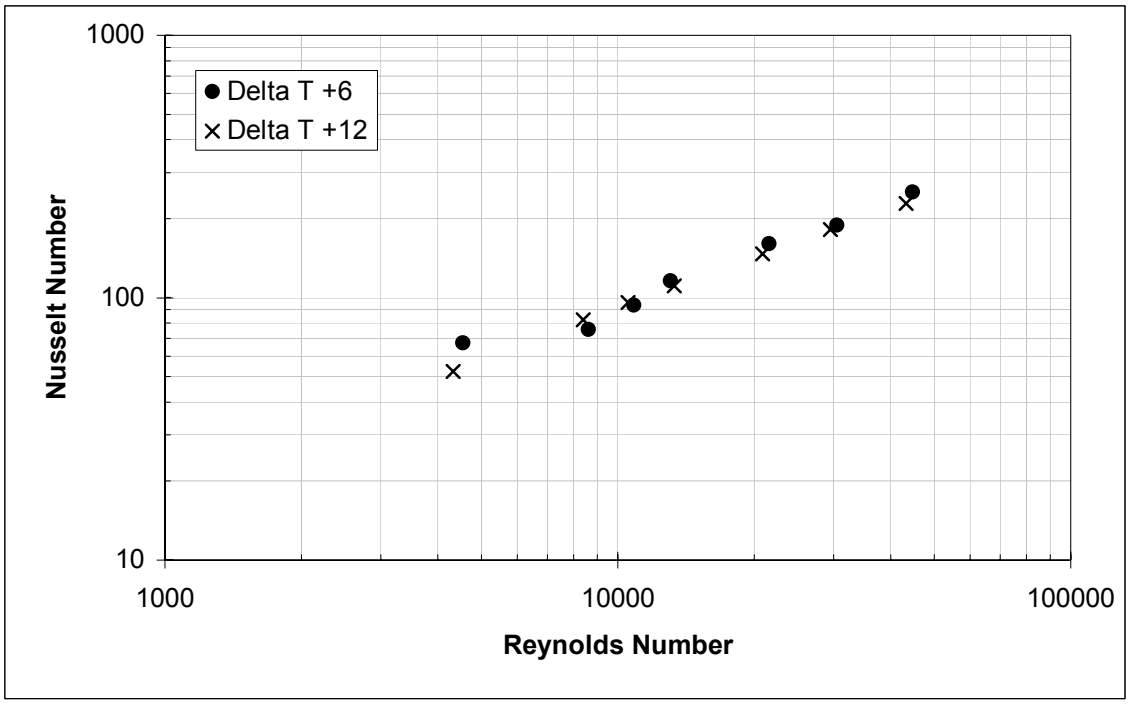

Figure 21. Nusselt number vs. Reynolds number for delta temperatures, case I

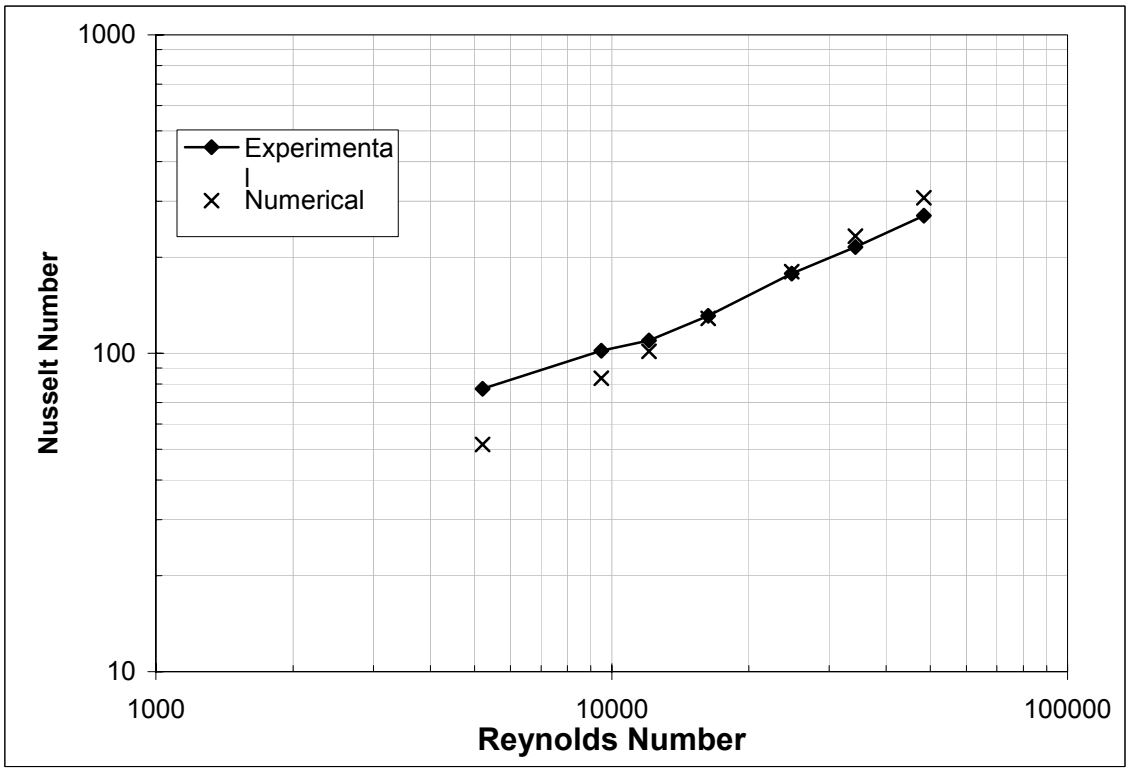

Figure 22. Nusselt number vs. Reynolds number for case II. Numerical data from Hamilton [2003] shown for comparison

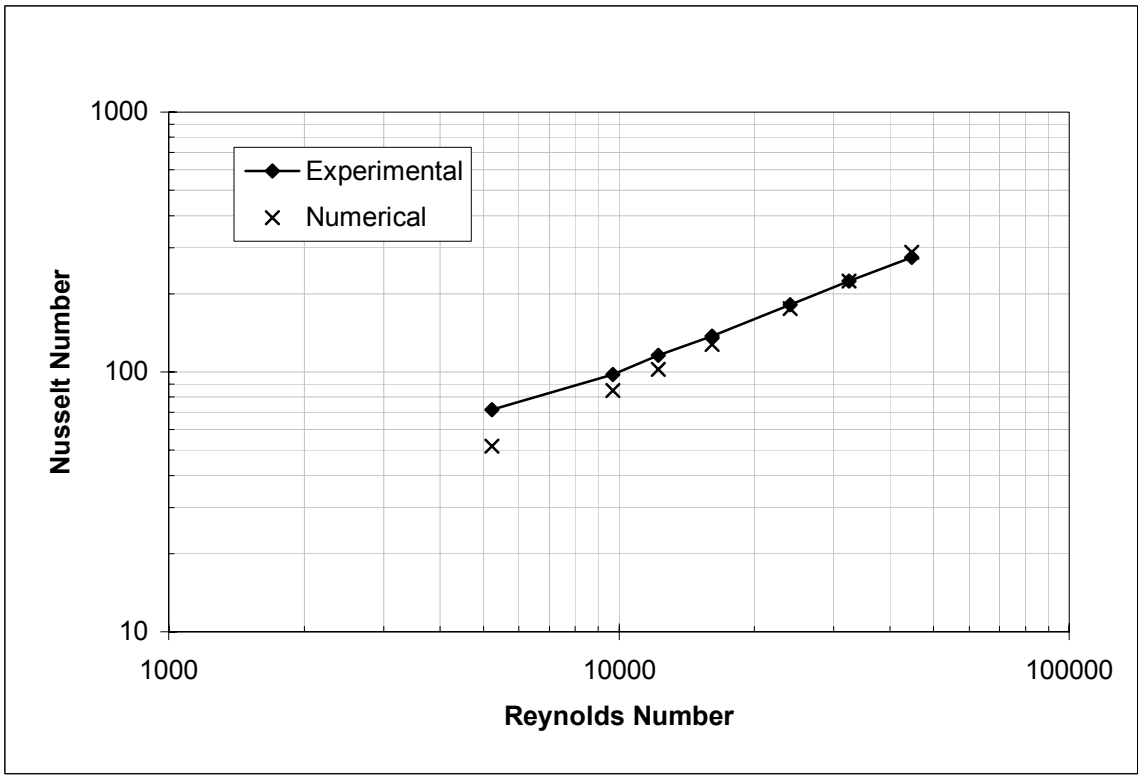

Figure 23. Nusselt number vs. Reynolds number for case II with turbulent generator. Numerical data from Hamilton [2003] shown for comparison

2. Row by Row Results

One characteristic of the methods used to construct this test apparatus, was the row-by-row analysis capability of determining the heat transfer coefficient and Nusselt number. Metzger [1982] concluded that the heat transfer coefficient increases until about the third to fifth row in the array, and then remains steady. The test runs and calculations completed with this experimental apparatus reveal similar results.

The steadying of the heat transfer coefficient and corresponding Nusselt number after about the third row of the heat exchanger array was evident in the cases where the flow into the test section had a fully developed velocity profile. The tests with the turbulence generators in place depicted a different behavior.

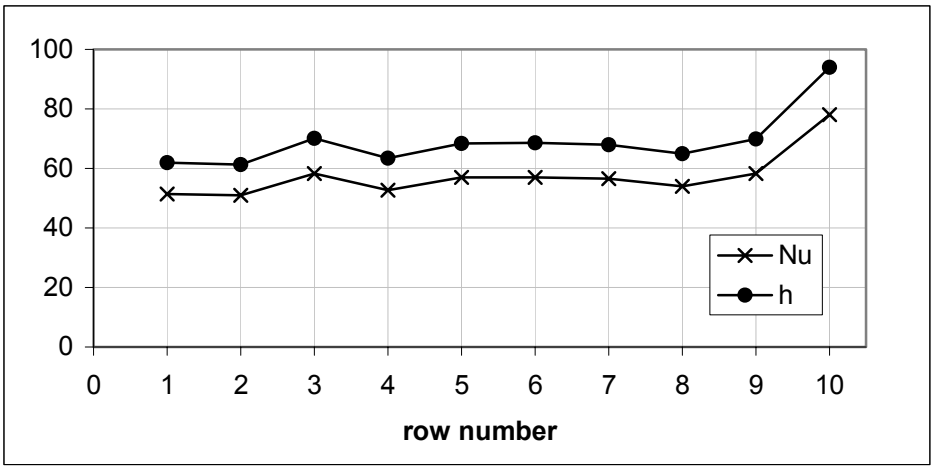

Figure 24. Row by row results of Nusselt number and heat transfer coefficient for case I delta T +6, Reynolds number ~4500

C. PRESSURE DROP AND FRICTION FACTOR RESULTS

To establish the correctness of the pressure transducer readings, an inclined manometer was used for comparison and the results were found to be within the published uncertainty from the manufacturer.

The comparison of the experimental and numerical results reveals an important difference. The numerical model pressure drop results across the heat exchanger test section indicated a larger pressure drop as compared to the experimental results (Figure 25).

In using the pressure drop to calculated friction factor, only the cases where the turbulence generators were not used could be discussed. The turbulence generators were installed downstream of the point where the high-pressure measurements were taken and therefore created artificial pressure losses that were not attributable to the heat exchanger test section.

As the friction factor results from the pressure drop, similar differences shown from the pressure drop comparison were repeated in the friction factor comparison.

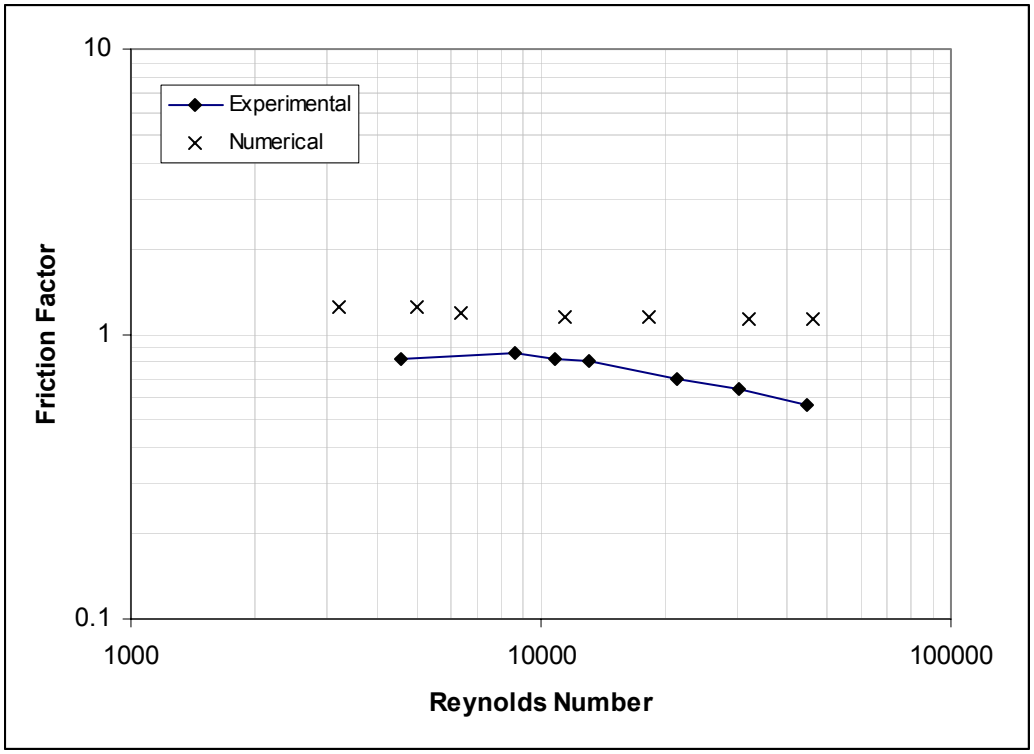

Figure 25. Friction factor vs. Reynolds number

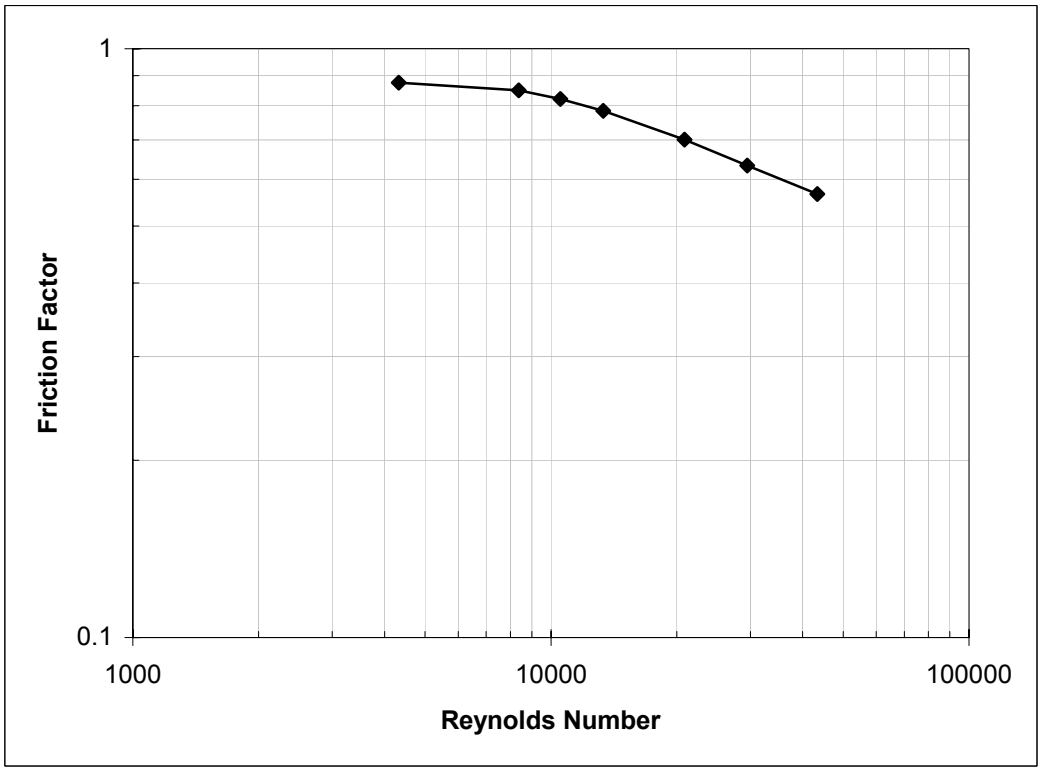

Figure 26. Friction factor vs. Reynolds number case I, no turbulence generator

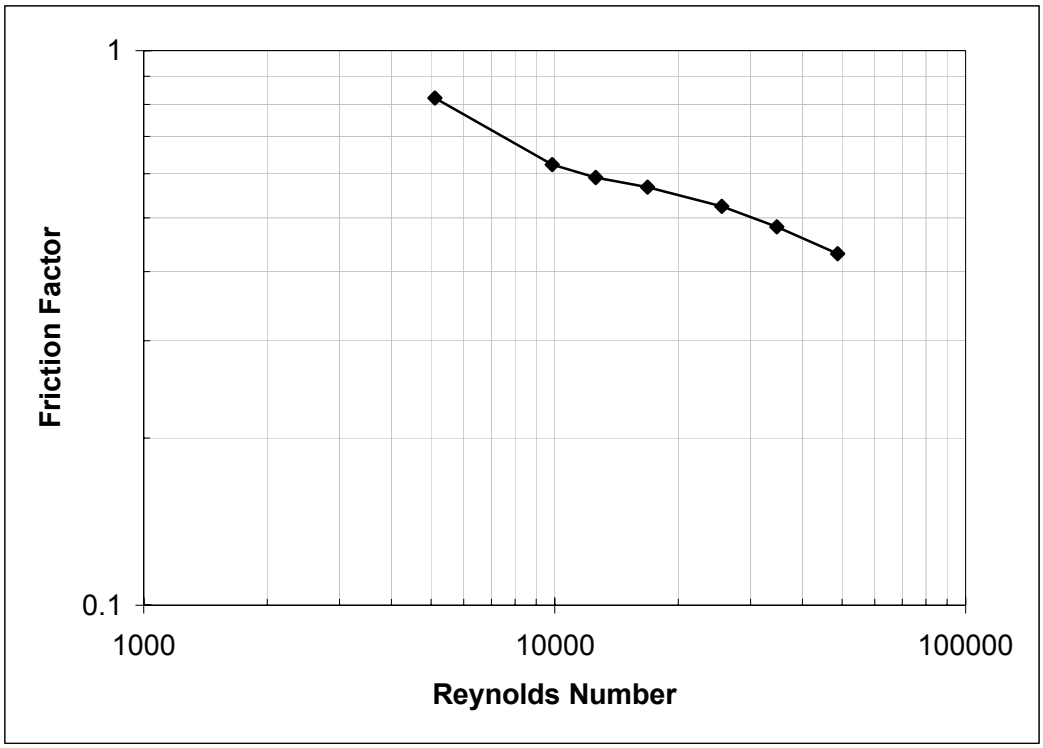

Figure 27. Friction factor vs. Reynolds number case II, no turbulence generation

D. HEAT TRANSFER COEFFICIENT

Standard measures for the effectiveness of a heat exchanger design use the amount of heat energy removed as a function of energy loss due to pressure drop. The design of a gas turbine engine uses bleed air from the compressor to provide the potential energy for cooling airflow through the turbine blades. In order to overcome the pressure of the gas exiting the combustor, the cooling air must come from the higher-pressure compressor stages. This bleeding of this high-pressure air lowers the efficiency of the engine.

The comparisons of the heat transfer coefficient verses the effective potential energy loss can be seen in Figures 28 and 29. As previously mentioned the turbulence generator test cannot be used due the inaccurately measured pressure drop data.

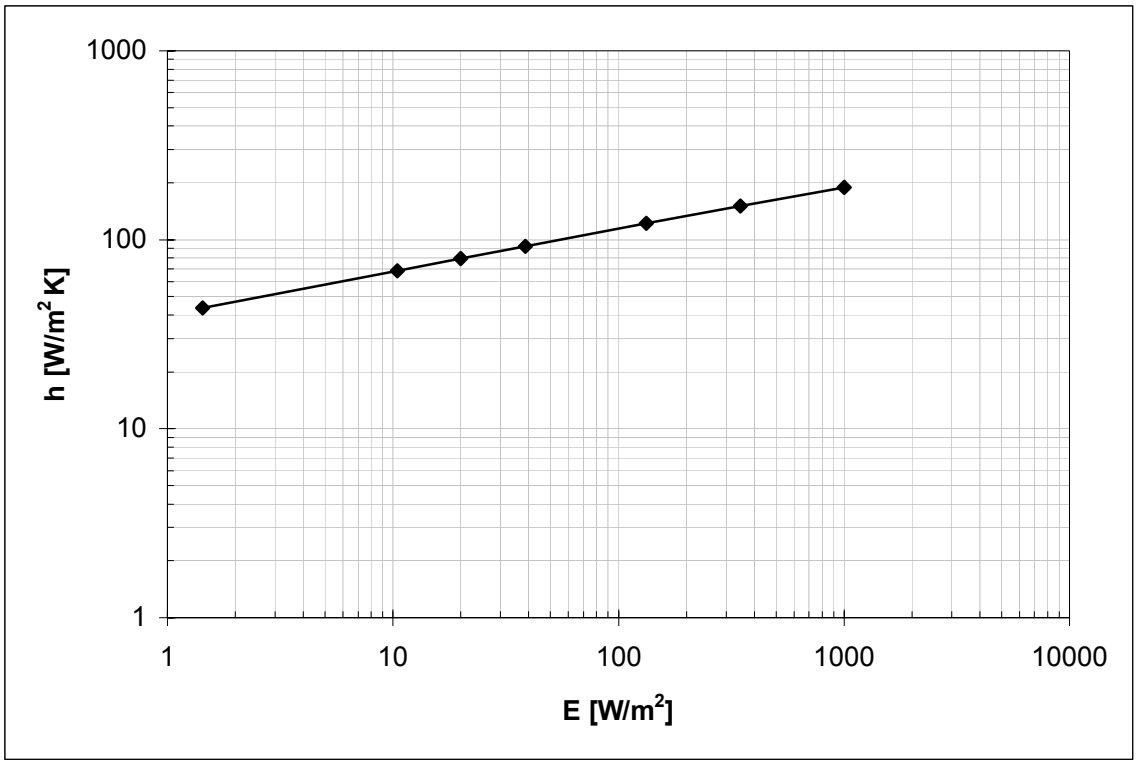

Figure 28. Heat transfer coefficient vs. frictional-power expenditure (E), case I, no turbulence

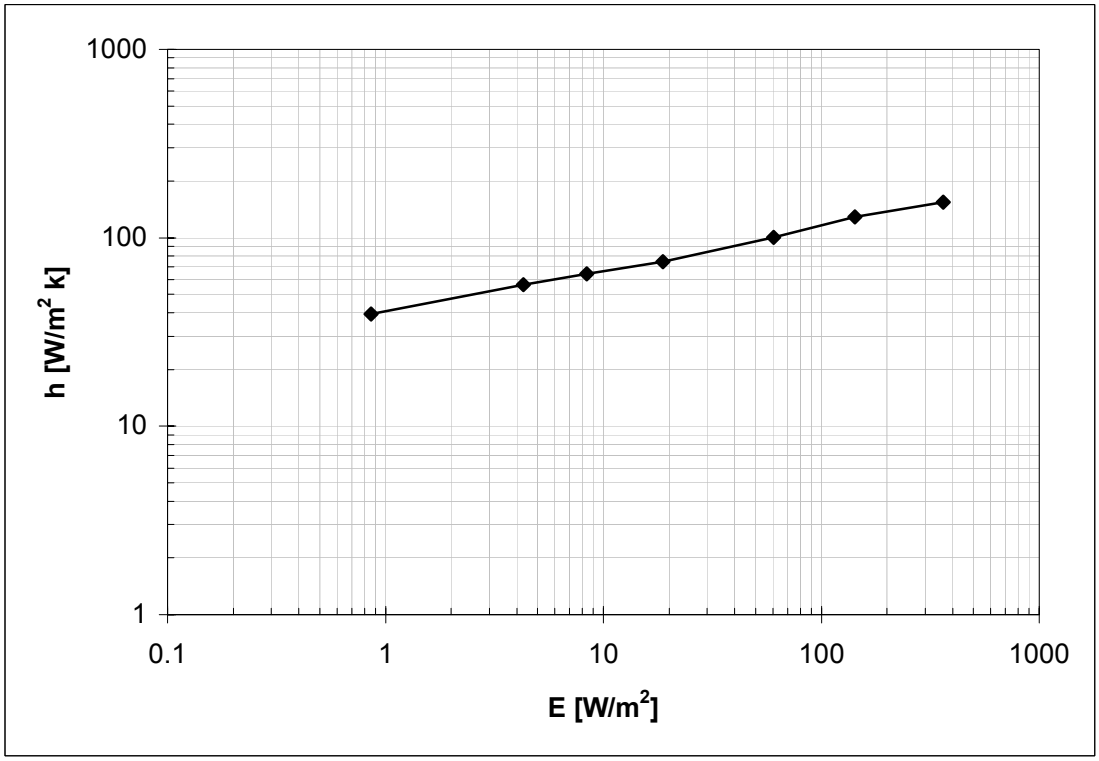

Figure 29. Heat transfer coefficient vs. frictional-power expenditure (E), case II, no turbulence

VI. CONCLUSIONS AND RECOMMENDATIONS

A. CONCLUSIONS

1. Nusselt Number

As seen from the previous section, the experimental apparatus gave good results as far as in the comparison of the Nusselt number to the numerical results. Further comparison with Metzger [1982] (Figure 30) shows similar results (Figure 31) in the row-by-row experimental results.

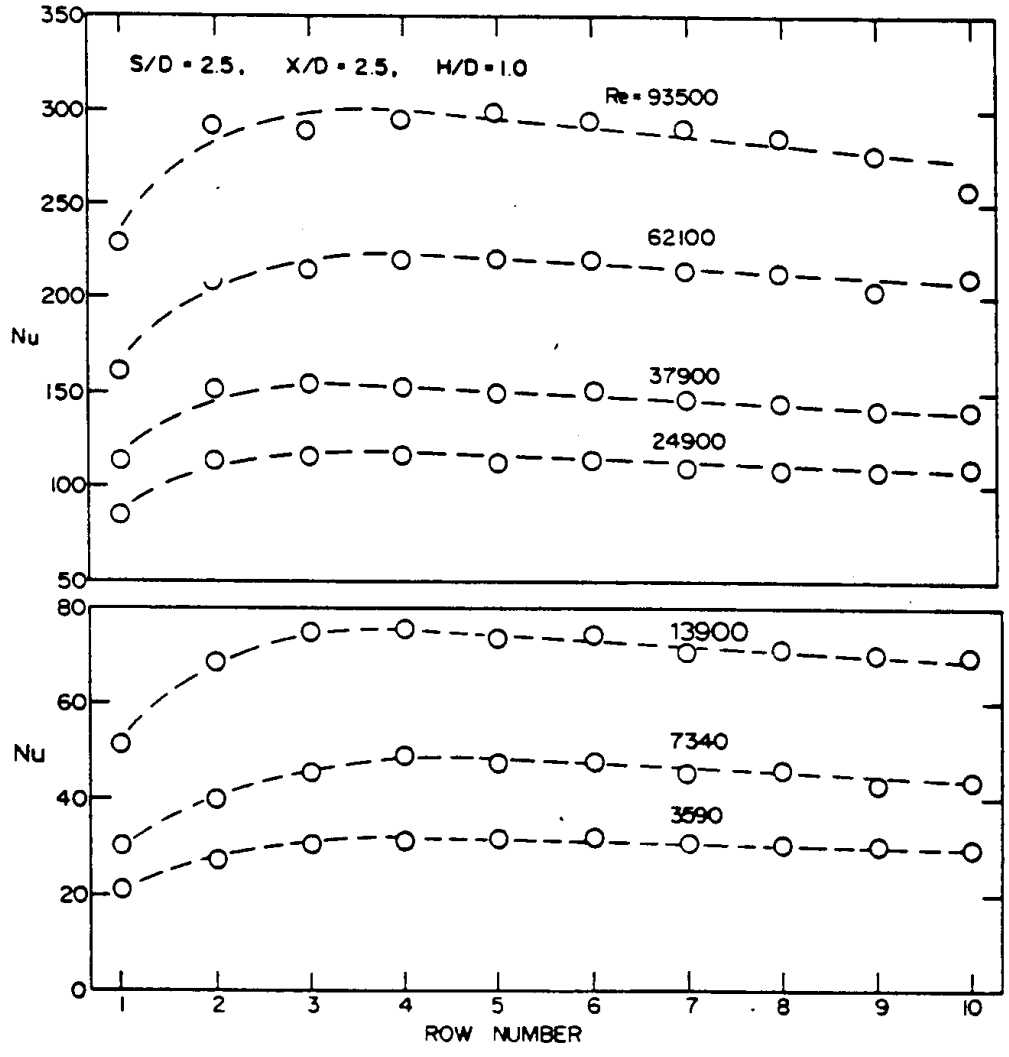

Fig. 4 Nu development for S/D = 2.5, X/D = 2.5

Figure 30. Reproduction from Metzger [1982]

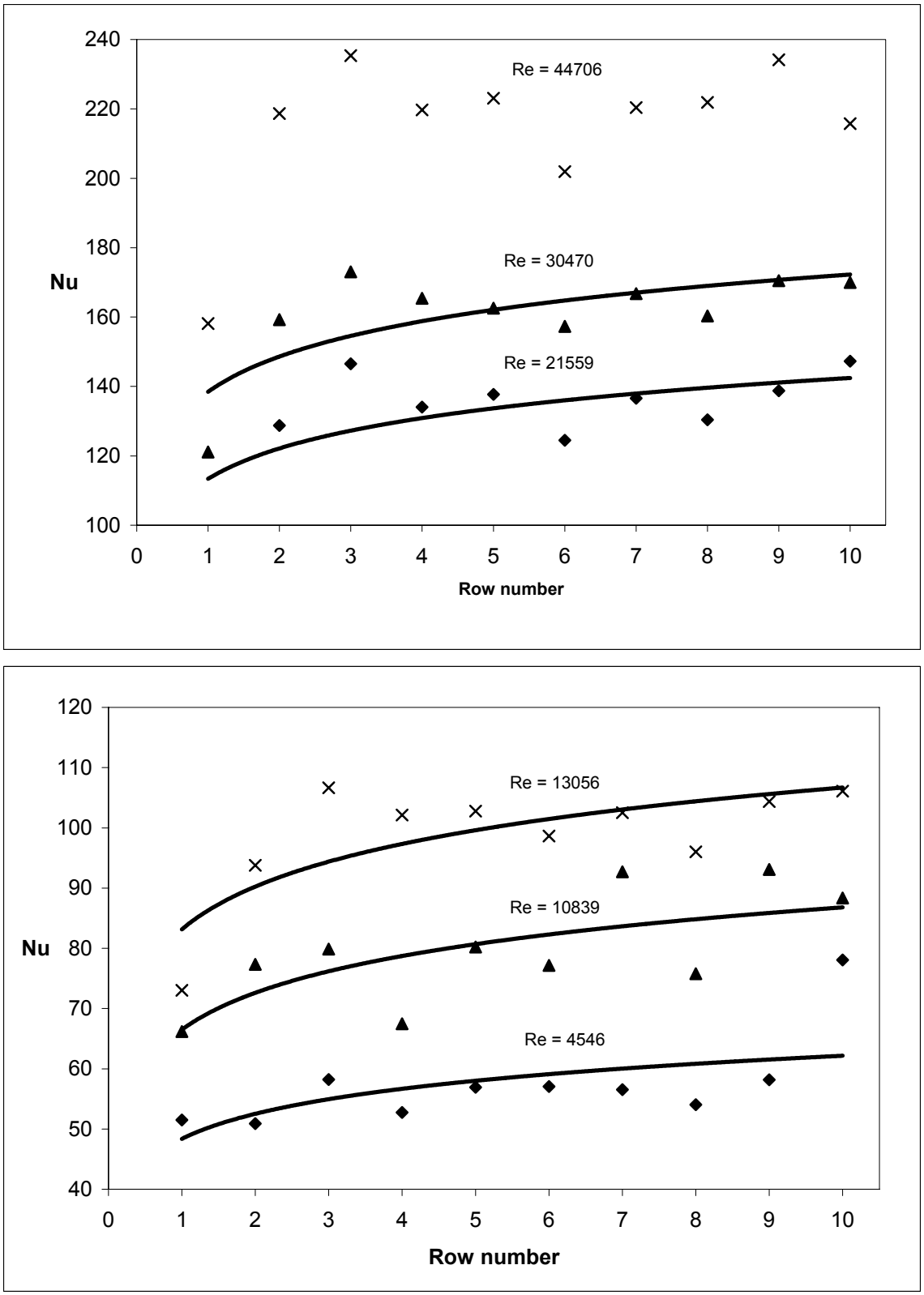

Figure 31. Row Nusselt number results with trend line for various Reynolds numbers, case I

2. Pressure Drop/Friction Factor

There were inconsistencies between the numerical and experimental results of the pressure drop across the test section for the round pins. This was most likely due to the limitations of the CFD turbulence model in simulating the separated region on the downstream side of the pins Figure 32. To remove any doubt as to the accuracy of the experimental data, the measured pressure drop was checked as previously mentioned with an inclined manometer. The check insured that measure pressure drop for the experimental setup was accurate. Because the friction factor is a function of the pressure drop, the same differences between the numerical and experimental solutions still exist.

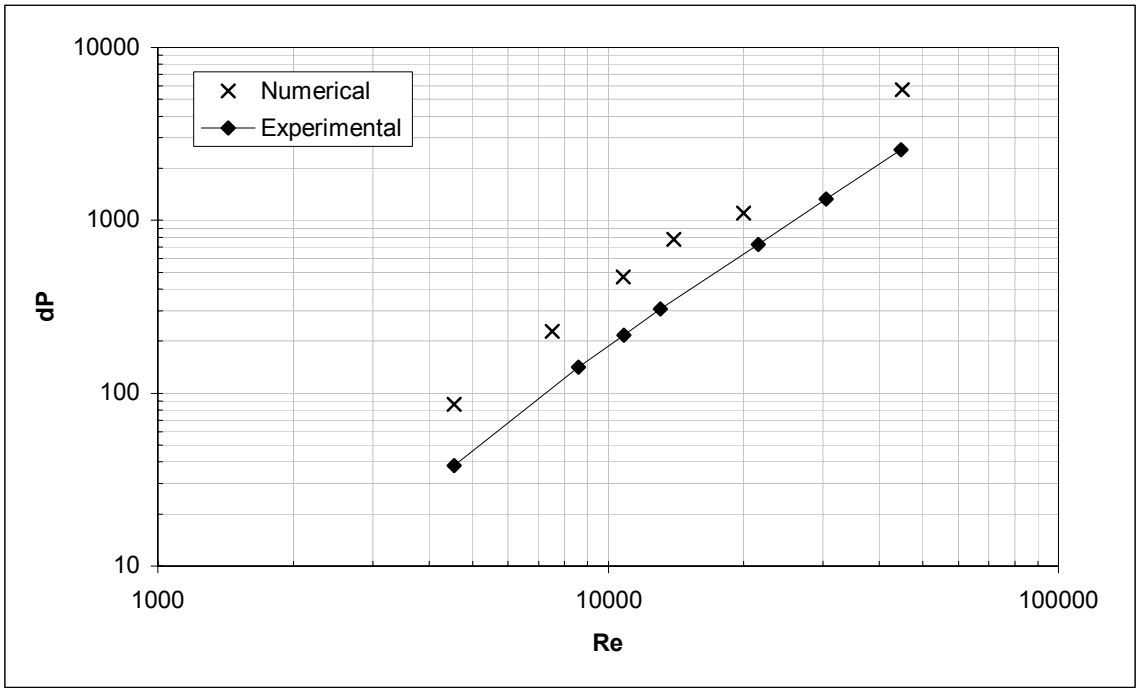

Figure 32. Comparisons of numerical to experimental pressure drop vs. Reynolds number for case I, no turbulence.

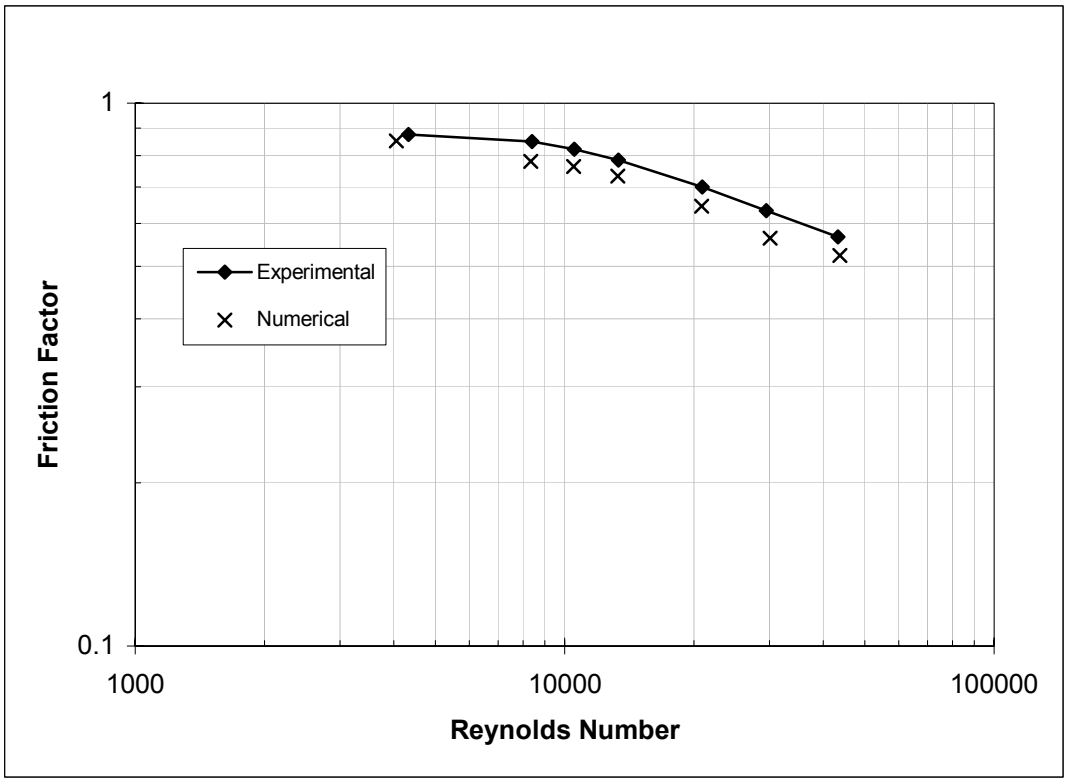

Figure 33. Comparison of friction factor vs. Reynolds number for case I. Numerical data from Hamilton [2003]

B. FUTURE WORK

1. Pin Configurations

There are a large number of possible pin shapes that can be tested with the current modular rig. This test apparatus was designed and built to be available for future work to develop a large database of experimental results.

2. Upgrades

There are changes that can be made to the visual control window of LABVIEW that would facilitate ease of use, visual impact and help in the data collection process. These changes are currently being implemented, but have no effect on the data already collected.

One desirable change to the data collection process would be to have the test apparatus and associated systems collect and store the zero flow data, the density pressure, the wall temperature settings and the zero offset data. That would remove the possibility of human error in entering the data into the MATLAB code.

One possible change to the entire test procedure could be to allow for individual control of the heaters. This would allow for adjusting the wall temperatures such that the temperature rise would be the same for all sections. This would allow for further study of the row heat transfer coefficients.

The flow straightening sections into and out from the mass flow meter are currently made from standard 2 ½inch, schedule 40, PVC pipe. The connections from the pipes to flow meter, required substantial attention during the assembly process. This additional attention is not within the objectives of a simple and easy to use design. Transparent piping with the appropriate connectors would add simplicity by aiding in the assembly and inspection process as well as add visual appeal.

A larger capacity blower could be used to reach higher mass flow rates. Reaching the higher flow rates would allow a comparison with a larger range of experimental and numerical solutions. The larger blower may be too powerful to be used with the current heaters and bypass system, so they may need to be upgraded as well.

The design of the heater test section has proven to be more than capable of the task at hand, however, there could be numerous changes and possibly several different test sections constructed and tested. The portability and sectional capability of the entire test apparatus allows it to be set up in various locations. The only external services required are a 220 VAC, 30-amp and a 110 VAC, 20-amp outlet. There will need to be a stable, level platform and enough square feet to accommodate about twenty-five feet by 5 feet.

THIS PAGE INTENTIONALLY LEFT BLANK

APPENDIX A

SAMPLE CALCULATIONS

1. Reynolds Number

$$\mathrm{Re}_{D_h} = \frac{\rho \bar{U} D_h}{\mu}$$

Where;

$$D_h = \frac{4V_{open}}{A_w} \quad \bar{U} = \frac{\dot{m}}{\rho \bar{A}}$$

Using Sutherland Law:

$$\mu = \mu_0 \left(\frac{T}{T_0} \right)^{3/2} \left(\frac{T_0 + S}{T + S} \right)$$

$$\text{where: } T_0 = 273K,\ S_{air} = 110.4K,\ \mu_0 = 1.71E-5\ \frac{kg}{m \bullet s}$$

For flow considerations;

$$A_w = 2\left(LW + HL - \frac{45\pi D^2}{4} \right) + 45\pi DH$$

$$V_{open} = LWH - 45\pi D^2 H$$

$$\bar{A} = \frac{V_{open}}{L}$$

$$\dot{Q} = \frac{\dot{m}}{\rho}$$

$$P = \rho RT$$

After substituting leads to;

$$\mathrm{Re}_{D_h} = \frac{P\dot{Q}D_h}{RT\bar{A}\mu}$$

With the voltages for the volumetric mass flow and pressure as well as the outlet temperature, the Reynolds number was calculated. One complete calculation is shown.

$$A_w = 2\left[(0.5m)(0.250m)+(0.033m)(0.5m)-11.25\pi(0.033m)^2\right]+45\pi(0.033m)^2 = 0.35998m^2$$

$$V_{open} = (0.5m)(0.25m)(0.033m)-\frac{45\pi(0.033m)^3}{4} = 0.0028549m^3$$

$$D_h = \frac{4\left(0.0028549m^3\right)}{\left(0.35998m^2\right)} = 0.037123m$$

$$\overline{A} = \frac{V_{open}}{L} = \frac{\left(0.0028549m^3\right)}{0.5m} = 0.0057098m^2$$

$$\dot{Q}\left[\tfrac{m^3}{s}\right] = \left(\dot{Q}_{VDC}[VDC]-\dot{Q}_{offset}[VDC]\right)0.0204\left[{}^{m^3}\!/_{s\bullet VDC}\right]$$
$$\dot{Q} = \left[(0.641VDC-0VDC)\,0.0204\,{}^{m^3}\!/_{s\bullet VDC}\right] = 0.013076\,{}^{m^3}\!/_{s}$$

$$P_{density} = P_{NOAA}-\left(P_{measured}-P_{offset}\right)$$
$$P_{density} = \left(30.13[inHg]\right)\left(3386.4\left[\frac{Pa}{inHg}\right]\right)-(1.67VDC-0.996VDC)\,6.25\left[\frac{inH_2O}{VDC}\right]\left(248.84\left[\frac{Pa}{inH_2O}\right]\right)$$
$$P_{density} = 100983[Pa]$$

$$P_{turbine} = P_{density}\left(1+\frac{\left(\frac{\dot{Q}}{A_{duct}}\right)^2}{2RT_{out}}\right)\Bigg/\left(1+\frac{\left(\frac{\dot{Q}}{A_{pipe}}\right)^2}{2RT_{out}}\right)$$

$$P_{turbine} = 101027Pa\left(1+\frac{\left(\frac{\left(0.013076\,{}^{m^3}\!/_{s}\right)}{(0.033m)(0.250m)}\right)^2}{2\left(287\,\frac{J}{kgK}\right)(300K)}\right)\Bigg/\left(1+\frac{\left(\frac{0.013076\,{}^{m^3}\!/_{s}}{\pi/4(0.062065m)^2}\right)^2}{2\left(287\,\frac{J}{kgK}\right)(300K)}\right) = 101039Pa$$

$$\mu = \left(1.71E-5\ \frac{kg}{m\bullet s}\right)\left(\frac{300.4K}{273K}\right)^{3/2}\left(\frac{273K+110.4K}{300.4K+110.4K}\right) = 0.0000184\,\frac{kg}{m\bullet s}$$

$$\mathrm{Re}_{D_h} = \frac{P_{turbine}\dot{Q}D_h}{RT\bar{A}\mu} = \frac{\left(101039Pa\right)\left(0.013076\,{}^{m^3}\!/_{s}\right)\left(0.037123m\right)}{\left(287\frac{J}{kgK}\right)\left(300.4K\right)\left(0.0057098m^2\right)\left(0.0000184\frac{kg}{m\bullet s}\right)} = 45489$$

3. Nusselt Number

$$Nu_{D_h} = \frac{\bar{h}_{array}D_h}{k}$$

Where

$$\bar{h}_{array} = \frac{Q}{A_{wetted}\Delta T_{lm}}$$

And

$$\Delta T_{lm} = \frac{\left(T_{wall} - T_{in}\right) - \left(T_{wall} - T_{out}\right)}{\ln\left(\frac{T_{wall} - T_{in}}{T_{wall} - T_{out}}\right)}$$

For heat transfer considerations, the side walls are not considered :

$$A_w = 2\left(LW - \frac{45\pi D^2}{4}\right) + 45\pi DH$$

$$A_w = 2\left[\left(0.5m\right)\left(0.250m\right) - 11.25\pi\left(0.033m\right)^2\right] + 45\pi\left(0.033m\right)^2 = 0.32698m^2$$

$$\Delta T_{lm} = \frac{\left(302K - 298.2K\right) - \left(302K - 300.8K\right)}{\ln\left(\frac{302K - 298.2K}{302K - 300.8K}\right)} = 2.3093K$$

$$\bar{h}_{array} = \frac{42.222W}{\left(0.32698m^2\right)\left(2.3093K\right)} = 55.916\frac{W}{m^2K}$$

$$Nu_{D_h} = \frac{\left(55.916\frac{W}{m^2K}\right)\left(0.037123m\right)}{0.02637\frac{W}{mK}} = 67.3$$

4. Friction Factor

$$f' = \frac{\Delta P_{array} D_h}{\frac{1}{2}\rho \bar{U}^2 L}$$

$$\bar{U} = \frac{\dot{Q}}{\bar{A}} = \frac{0.013076\,{}^{m^3}\!/_{s}}{0.0057098 m^2} = 2.255\,{}^{m}\!/_{s}$$

$$\rho = \frac{P_{turbine}}{RT} = \frac{101039 Pa}{287\frac{J}{kgK}(300.4K)} = 1.1704\frac{kg}{m^3}$$

$$\Delta P_{array} = P_{measured} - P_{offset}$$

$$\Delta P_{array} = (1.022VDC - 0.996VDC)6.25\left[\frac{inH_2O}{VDC}\right]\left(248.84\left[\frac{Pa}{inH_2O}\right]\right) = 40.46Pa$$

$$f' = \frac{(40.46Pa)(0.037123m)}{\frac{1}{2}\left(1.1704\,{}^{kg}\!/_{m^3}\right)\left(2.255\,{}^{m}\!/_{s}\right)^2(0.500m)} = 0.8139$$

5. Frictional Power Expenditure (E)

$$E = \frac{\dot{m}\Delta P}{\rho A_w} = \frac{\dot{Q}\Delta P}{A_w}$$

$$E = \frac{\left(0.013076\,{}^{m^3}\!/_{s}\right)(40.46Pa)}{\left(0.32698m^2\right)} = 1.618\frac{W}{m^2}$$

APPENDIX B

UNCERTAINTY ANALYSIS

1. Reynolds Number

The Reynolds number is a function of pressure, volumetric flow rate, physical dimensions and temperature. The characteristic dimensions, $\bar{A}$ and D_h, were assumed to have negligible uncertainty.

$$\mathrm{Re}_{D_h} = \frac{P\dot{Q}D_h}{RT\bar{A}\mu}$$

$$\frac{\omega \mathrm{Re}_{D_h}}{\mathrm{Re}_{D_h}} = \sqrt{\left(\frac{\omega D_h \partial \mathrm{Re}_{D_h}}{\mathrm{Re}_{D_h}\partial D_h}\right)^2 + \left(\frac{\omega \bar{A} \partial \mathrm{Re}_{D_h}}{\mathrm{Re}_{D_h}\partial \bar{A}}\right)^2 + \left(\frac{\omega P \partial \mathrm{Re}_{D_h}}{\mathrm{Re}_{D_h}\partial P}\right)^2 + \left(\frac{\omega \dot{Q} \partial \mathrm{Re}_{D_h}}{\mathrm{Re}_{D_h}\partial \dot{Q}}\right)^2 + \left(\frac{\omega R \partial \mathrm{Re}_{D_h}}{\mathrm{Re}_{D_h}\partial R}\right)^2 + \left(\frac{\omega T \partial \mathrm{Re}_{D_h}}{\mathrm{Re}_{D_h}\partial T}\right)^2 + \left(\frac{\omega \mu \partial \mathrm{Re}_{D_h}}{\mathrm{Re}_{D_h}\partial \mu}\right)^2}$$

$$\frac{\partial \mathrm{Re}_{D_h}}{\mathrm{Re}_{D_h}\partial P} = \left(\frac{\dot{Q}D_h}{RT\mu}\right)\left(\frac{RT\mu}{P\dot{Q}D_h}\right) = \frac{1}{P}$$

$$\frac{\partial \mathrm{Re}_{D_h}}{\mathrm{Re}_{D_h}\partial \dot{Q}} = \left(\frac{PD_h}{RT\mu}\right)\left(\frac{RT\mu}{P\dot{Q}D_h}\right) = \frac{1}{\dot{Q}}$$

$$\frac{\partial \mathrm{Re}_{D_h}}{\mathrm{Re}_{D_h}\partial T} = \left(-\frac{P\dot{Q}D_h}{RT^2\mu}\right)\left(\frac{RT\mu}{P\dot{Q}D_h}\right) = -\frac{1}{T}$$

With uncertainty for D_h, $\bar{A}$, μ, and R considered negligible leads to:

$$\frac{\omega \mathrm{Re}_{D_h}}{\mathrm{Re}_{D_h}} = \sqrt{\left(\frac{\omega P}{P}\right)^2 + \left(\frac{\omega \dot{Q}}{\dot{Q}}\right)^2 + \left(\frac{\omega T}{T}\right)^2}$$

Flow rate uncertainty where the coefficients C_1 and C_2 were determined previously:

$$\omega\dot{Q} = \frac{C_1}{C_2}V_f = \frac{0.0002}{0.0106}V_f$$

$$\frac{\omega \dot{Q}}{\dot{Q}} = \sqrt{\left(\frac{\Delta C_1}{C_1}\right)^2 + \left(\frac{\Delta C_2}{C_2}\right)^2 + \left(\frac{\Delta V_f}{V_f}\right)^2}$$

The uncertainty in the volumetric flow rate for the flow meter was determined to be 0.11% as stated by the manufacturer. This was the calibration accuracy of the equipment used by the manufacturer to calibrate the flow meter. The flow meter transmitter calibration sheet shows a varying uncertainty of 0.03 VDC maximum. This 0.03 VDC error was considered the predominate factor in the flow rate measurement. Therefore the uncertainties associated with C_1 and C_2 were determined to be negligible.

$$\frac{\omega \dot{Q}}{\dot{Q}} = \left(\frac{\omega V_f}{V_f}\right) = \left(\frac{0.03VDC}{V_f}\right)$$

The uncertainty of the pressure transducer was stated by the manufacturer to be 0.25% of the full-scale voltage. The full-scale voltage for the pressure transducer was 5 VDC. If the pressure transducer were used at full scale, then the error would have been 41 Pascal. This was based on 1.0025 times the full-scale voltage of 5 VDC, then using the linear trend line equation previously discussed.

$$\frac{\omega P}{P} = \left(\frac{41Pa}{P}\right)$$

The thermocouples were assumed to have an uncertainty of $\pm 0.5^{\circ}$. This is the standard for 'E' type thermocouples.

$$\frac{\omega T}{T} = \left(\frac{0.5K}{T}\right)$$

After substituting uncertainties leads to:

$$\frac{\omega \,\mathrm{Re}_{D_h}}{\mathrm{Re}_{D_h}} = \sqrt{\left(\frac{41Pa}{P}\right)^2 + \left(\frac{0.03VDC}{V_f}\right)^2 + \left(\frac{0.5K}{T}\right)^2}$$

For the maximum and minimum Reynolds Numbers from a case I test:

$$\frac{\omega \mathrm{Re}_{D_h}}{\mathrm{Re}_{D_h}} = \sqrt{\left(\frac{41Pa}{100725Pa}\right)^2 + \left(\frac{0.03VDC}{0.635VDC}\right)^2 + \left(\frac{0.5K}{306.15K}\right)^2} = 0.04727$$

$$\approx 4.73\% @ \mathrm{Re}_{D_h} = 3997$$

$$\approx 0.503\% @ \mathrm{Re}_{D_h} = 40092$$

2. Nusselt Number

The uncertainty in the Nusselt number lies mainly with the energy transferred from the heaters. The energy from the individual heaters varied, so the overall energy transferred for the array for the test run was used.

$$Nu_{D_h} = \frac{\bar{h}_{array} D_h}{k}$$

$$\bar{h}_{array} = \frac{Q}{A_{wetted} \Delta T_{lm}}$$

$$\Delta T_{lm} = \frac{\left(T_{wall} - T_{in}\right) - \left(T_{wall} - T_{out}\right)}{\ln\left(\frac{T_{wall} - T_{in}}{T_{wall} - T_{out}}\right)}$$

After substituting and assuming that the uncertainties from A_{wetted}, D_h, and k are negligible:

$$\frac{\omega Nu_{D_h}}{Nu_{D_h}} = \sqrt{\left(\frac{\omega Q \partial Nu_{D_h}}{Nu_{D_h} \partial Q}\right)^2 + \left(\frac{\omega \Delta T_{lm} \partial Nu_{D_h}}{Nu_{D_h} \partial \Delta T_{lm}}\right)^2}$$

$$\frac{\partial Nu_{D_h}}{Nu_{D_h} \partial Q} = \frac{1}{Q}$$

$$\frac{\partial Nu_{D_h}}{Nu_{D_h} \partial \Delta T_{lm}} = \frac{1}{\Delta T_{lm}}$$

$$\frac{\omega Nu_{D_h}}{Nu_{D_h}} = \sqrt{\left(\frac{\omega Q}{Q}\right)^2 + \left(\frac{\omega \Delta T_{lm}}{\Delta T_{lm}}\right)^2}$$

From the knowledge that the test runs lasted approximately 20 minutes and each on/off cycle was 8.547 seconds, the uncertainty was determined to be:

$$\frac{\omega Q}{Q} = \frac{8.547[\text{sec}][1\,\text{min}]}{20[\text{min}][60\,\text{sec}]Q} = \frac{0.0071}{Q}$$

The uncertainty of the thermocouples was determined to be 0.5K as previously described.

$$\frac{\omega \Delta T_{lm}}{\Delta T_{lm}} = \frac{0.5K}{\Delta T_{lm}}$$

$$\frac{\omega Nu_{D_h}}{Nu_{D_h}} = \sqrt{\left(\frac{0.0071}{Q}\right)^2 + \left(\frac{0.5K}{\Delta T_{lm}}\right)^2}$$

$$\frac{\omega Nu_{D_h}}{Nu_{D_h}} = \sqrt{\left(\frac{0.0071}{511.22}\right)^2 + \left(\frac{0.5}{8.0781}\right)^2} = 0.0619$$

$$\approx 6.19\% @ Nu_{D_h} = 233$$

$$\approx 7.06\% @ Nu_{D_h} = 55.4$$

3. Friction Factor

$$f' = \frac{\Delta P_{array} D_h}{\frac{1}{2}\rho \bar{U}^2 L}$$

$$\bar{U} = \frac{\dot{Q}}{\bar{A}} \qquad \rho = \frac{P_{turbine}}{RT} \qquad \Delta P_{array} = \Delta P_{measured} - \Delta P_{offset}$$

After substituting:

$$f' = \frac{\left(\Delta P_{measured} - \Delta P_{offset}\right) D_h}{\frac{1}{2}\frac{P_{turbine}}{RT_{out}}\left(\frac{\dot{Q}}{\bar{A}}\right)^2 L}$$

The uncertainties for $D_h, \bar{A}, L,$ and R were considered negligible, therefore:

$$\frac{\omega f'}{f'} = \sqrt{\left(\frac{\omega \Delta P_{measured}\,\partial f'}{f'\,\partial \Delta P_{measured}}\right)^2 + \left(\frac{\omega \Delta P_{offset}\,\partial f'}{f'\,\partial \Delta P_{offset}}\right)^2 + \left(\frac{\omega P_{turbine}\,\partial f'}{f'\,\partial P_{turbine}}\right)^2 + \left(\frac{\omega \dot{Q}\,\partial f'}{f'\,\partial \dot{Q}}\right)^2 + \left(\frac{\omega T_{out}\,\partial f'}{f'\,\partial T_{out}}\right)^2}$$

$$\frac{\partial f'}{f'\,\partial \dot{Q}} = \frac{-2}{\dot{Q}}$$

$$\frac{\partial f'}{f'\partial T} = \frac{1}{T}$$

$$\frac{\partial f'}{f'\partial P_{turbine}} = \frac{-1}{P_{turbine}}$$

$$\frac{\partial f'}{f'\partial \Delta P_{measured}} = \frac{1}{\Delta P_{measured}}$$

$$\frac{\omega f'}{f'} = \sqrt{\left(\frac{\omega \Delta P_{measured}}{\Delta P_{measured}}\right)^2 + \left(\frac{-1\omega P_{turbine}}{P_{turbine}}\right)^2 + \left(\frac{-2\omega \dot{Q}}{\dot{Q}}\right)^2 + \left(\frac{\omega T_{out}}{T_{out}}\right)^2}$$

The uncertainty for $\Delta P_{measured}$ was determined previously to be 41 Pa. The uncertainty of ΔP_{offset} was based on the voltage measurement at zero flow conditions. However this was recorded and the conversion from volts to pressure was adjusted. The uncertainty for ΔP_{offset} was considered zero because it was known. $P_{turbine}$ was measured at the onset of each test run. It was subjected to be the same uncertainty as previously described. The uncertainty of $\Delta P_{measured}$ was determined from the smallest measurable pressure difference (1.25Pa) on an inclined manometer. The manometer was used to measure the pressure differential with equipment that could be calibrated. The temperature and flow rate uncertainties were the same as previously described. The flow rate uncertainty is repeated below.

$$\frac{\omega \dot{Q}}{\dot{Q}} = \left(\frac{\omega V_f}{V_f}\right) = \left(\frac{0.03VDC}{V_f}\right)$$

$$\frac{\omega f'}{f'} = \sqrt{\left(\frac{1.25Pa}{\Delta P_{measured}}\right)^2 + \left(\frac{41Pa}{P_{turbine}}\right)^2 + \left(\frac{2(0.03VDC)}{V_f}\right)^2 + \left(\frac{0.5K}{T_{out}}\right)^2}$$

For a case I test run at the maximum and minimum flow rates:

$$\frac{\omega f'}{f'} = \sqrt{\left(\frac{1.25Pa}{39.028Pa}\right)^2 + \left(\frac{41Pa}{100725Pa}\right)^2 + \left(\frac{2(0.03VDC)}{0.635}\right)^2 + \left(\frac{0.5K}{306.15}\right)^2} = 0.0998$$

$$\approx 9.98\% @ f' = 1.0252$$

$$\approx 0.967\% @ f' = 0.6622$$

APPENDIX C

DETAILS OF DESIGN

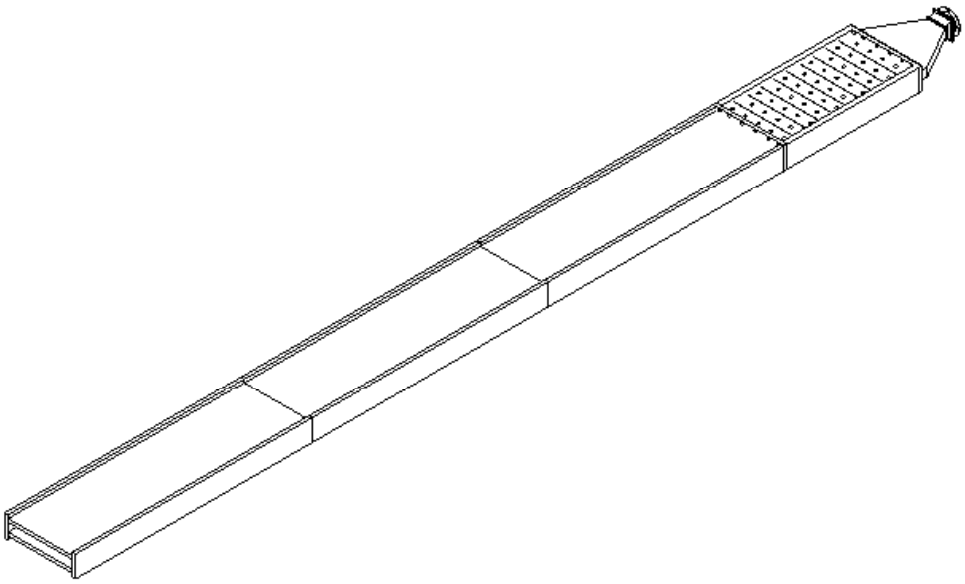

Figure 34. CAD of inlet, test section, and exit duct assembly

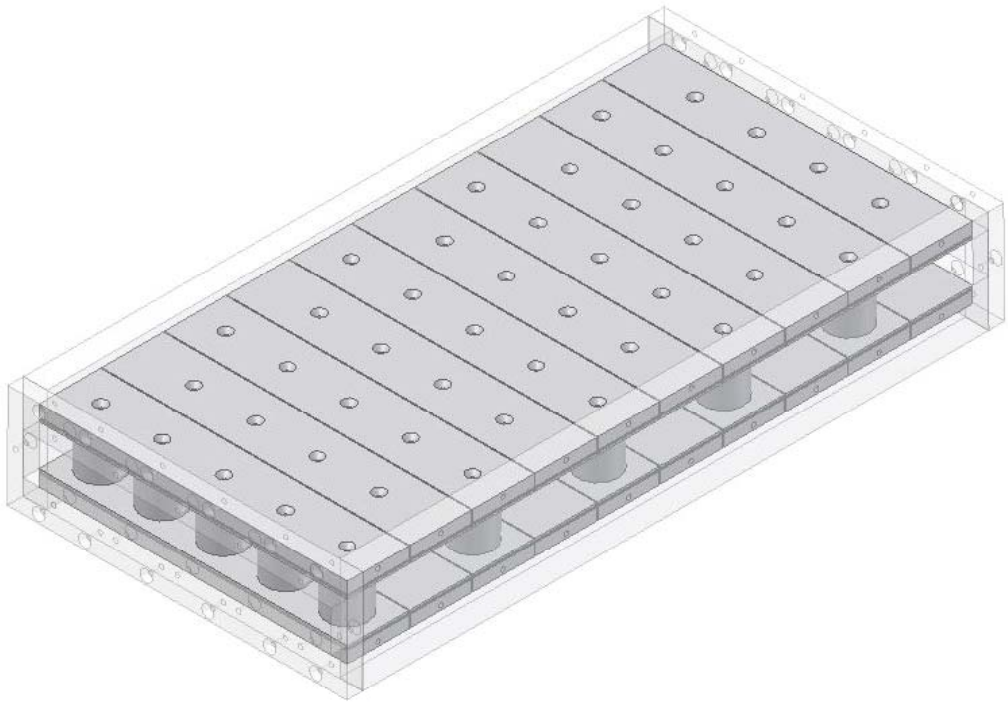

Figure 35. CAD of test section with 33 mm pins

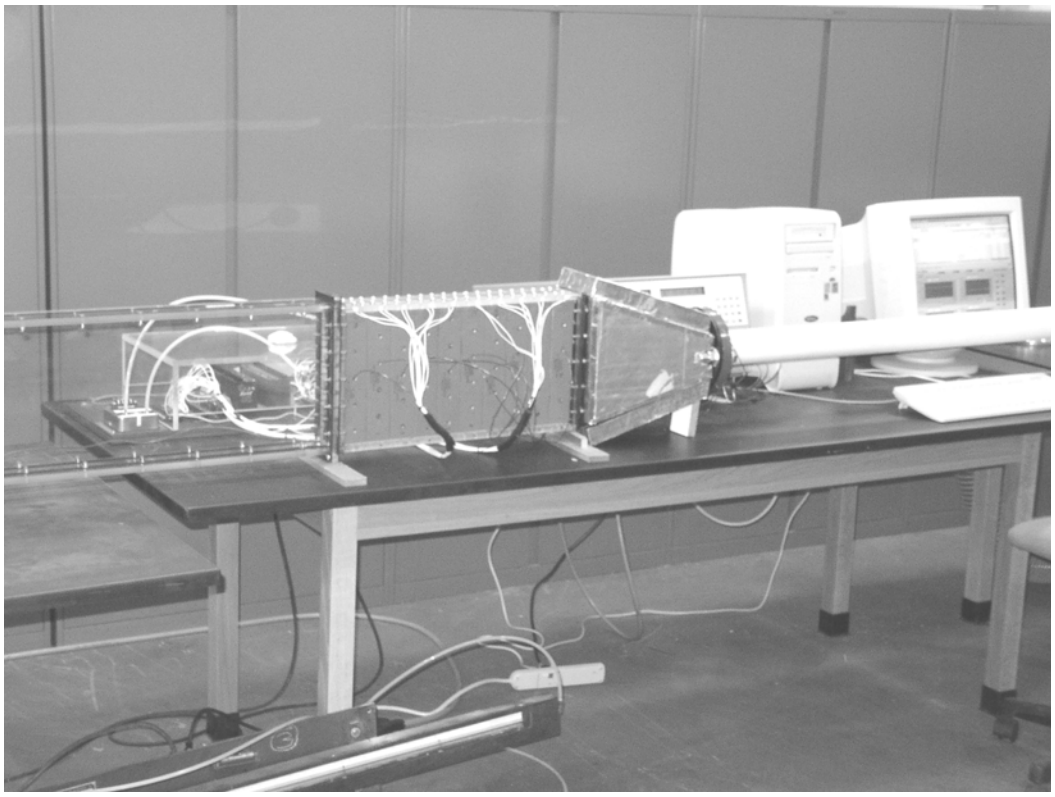

Figure 36. Completed assembly of Heat Exchanger Test Section

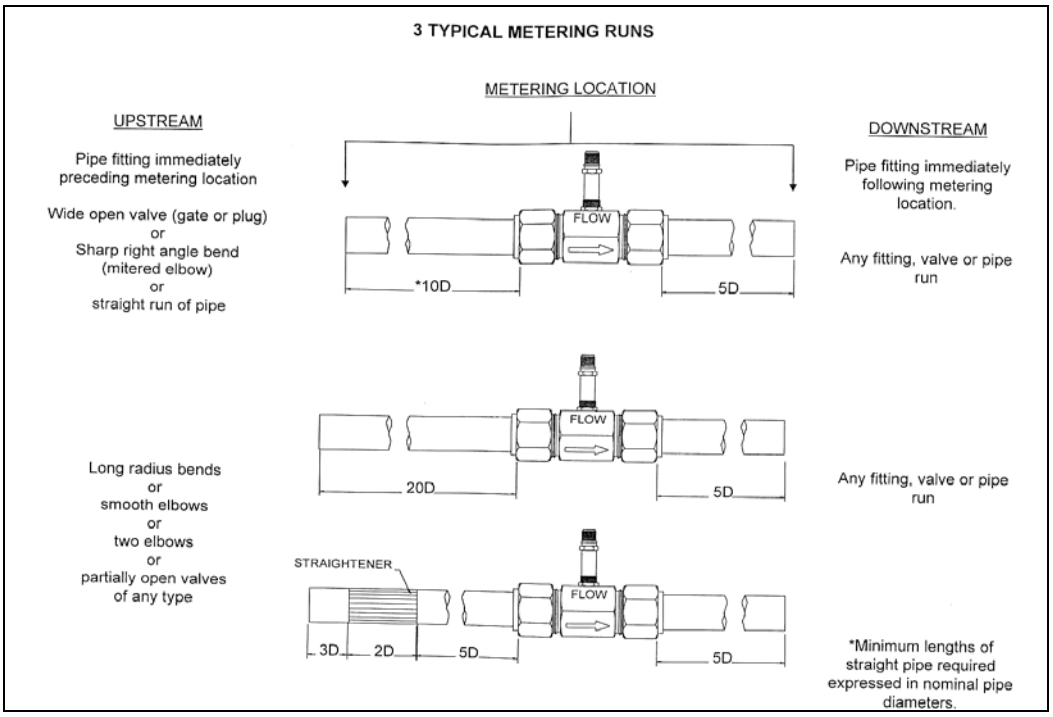

Figure 37. Flow Meter Installation Requirements

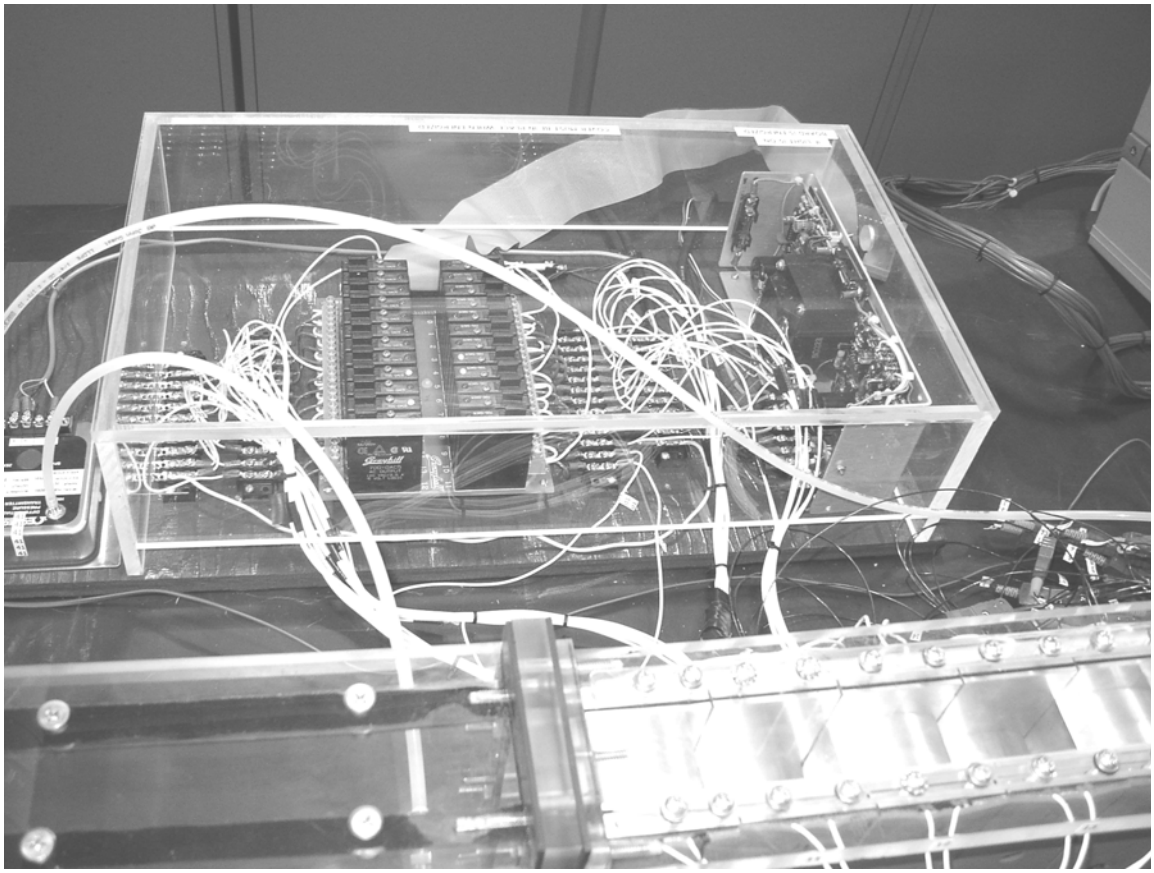

Figure 38. Relay board enclosure

THIS PAGE INTENTIONALLY LEFT BLANK

APPENDIX D

PARTS LIST

1. Blower: Busch; Samos Regenerative Blower model #FBC 3388-6
   Capacities: 135 CFM

Figure 39. Typical Samos Regenerative Blower

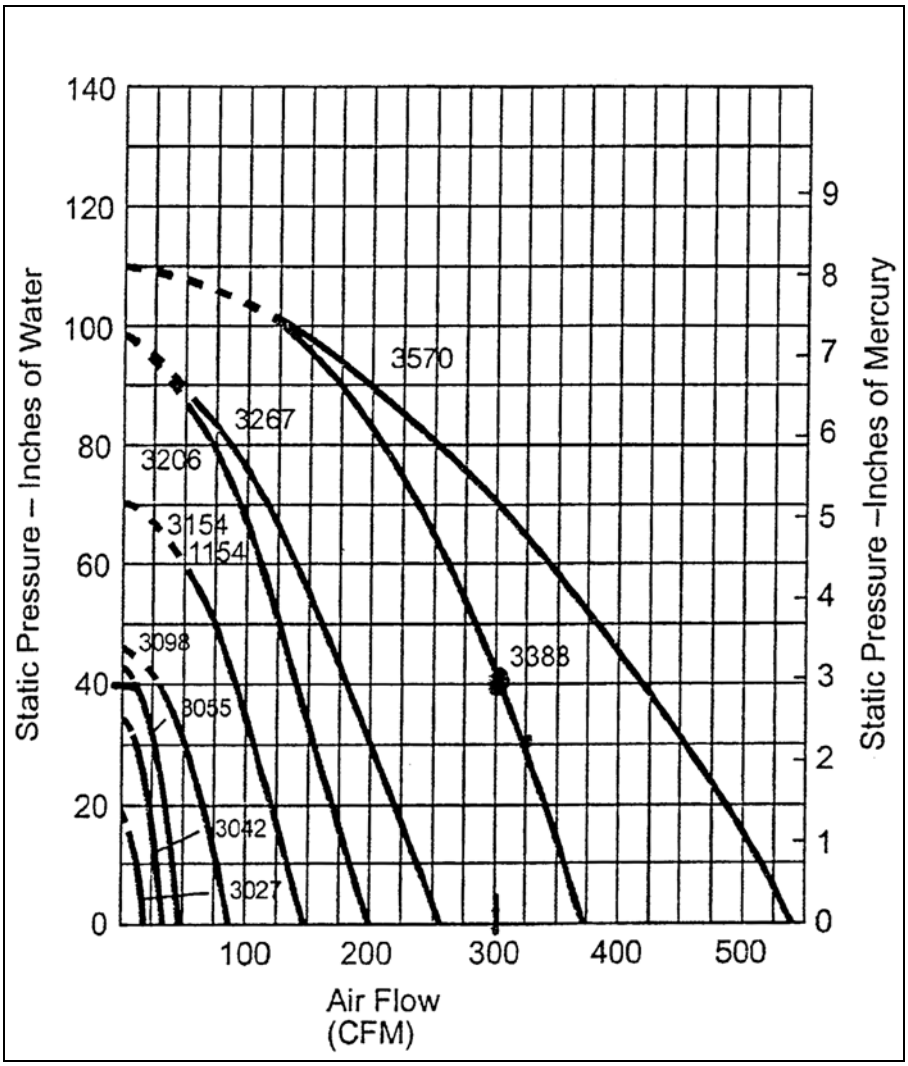

Figure 40. Blower Pump Curve, Manufacturer Data

2. Mass Flow meter: Omega FTB 940
   Capabilities: 25 - 450 ACFM

Figure 41. Similar Mass Flow Meter with Transducer

3. Heaters: Watlow Silicone Rubber, Wire wound heater, model 020050C1
   120 Volts AC, 50 Watts, 50 mm by 250 mm

4. Thermocouples: Omega E type; part # 5SRTC-KK-E-30-36

5. Thermally Conductive Epoxy: Omega, OB-200

6. Differential Pressure Transducer: Omega part # PX653-50D5V

7. Relay board and Relays: Grayhill; 24 channel rack, # 70GRCQ24
   Grayhill; G5 Modules, #70G-OAC5

8. Power meter: Brand Electronics, Model 20-1850/CI

Figure 42. Brand Electronics Power Meter

APPENDIX E

EQUIPMENT LIST

- Pentium III computer, monitor etc.
- PC to HP 3852A interface card
- Hewlett Packard 3852A data acquisition unit
- HP3852A control modules
- Grayhill Relay board with HP interface ribbon cable
- Constant voltage supply
- Brand Electric power meter
- National Instruments LABVIEW software

THIS PAGE INTENTIONALLY LEFT BLANK

LIST OF REFERENCES

Arora, S.C., and Abdel-Messeh, W., Pressure Drop and Heat Transfer Characteristics of Circular and Oblong Low Aspect Ratio Pin Fins, AGARD Conference Proceedings, pp.4-1-4-15, 1985.

Avallone, E. A. and Baumeister III, T., editors, *Marks' Standard Handbook for Mechanical Engineers*, McGraw-Hill, Inc., 10th Ed., 1996.

Chyu, M. K., *Effects of Perpendicular Flow Entry on Convective Heat/Mass Transfer from Pin-Fin Arrays*, ASME Journal of Heat Transfer, Vol. 121, 1999, pp. 668-674.

Hamilton, L.J., *Numerical Analysis of the Performance of a Staggered Cross-Pin Array Heat exchanger*, Naval Postgraduate School, Monterey, California, 2003.

Holman, J. P., *Experimental Methods For Engineers*, McGraw-Hill, Inc., 6th Ed., 1994.

Incropera, F. P. and DeWitt, D. P., *Introduction to Heat Transfer*, John Wiley and Sons, New York, NY, 3rd Ed., 1985.

Kays, W. M. and London, A. L., *Compact Heat Exchangers*, McGraw-Hill, Inc., 3rd Ed., 1984.

Linberg, M. R., *Mechanical Engineering Reference Manual for the PE Exam*, Professional Publications, Inc., Belmont, California, 11th Ed., 2001.

Metzger, D.E., *Developing Heat Transfer in Rectangular Ducts With Staggered Arrays of Short Pin Fins*, ASME Journal of Heat Transfer, Vol. 104, 1982, pp. 700-706.

Shah, R. K., *Progress in the Numerical Analysis of Compact Heat Exchanger Surfaces*, Advances in Heat Transfer, Vol. 34, Academic Press, 2001, pp. 363-443.

Weills, N. D. and Ryder, E. A., *Thermal Resistance Measurements of Joints Formed Between Stationary Metal Surfaces*, Transactions of the ASME, April 1949, pp. 259-267.

White, F. M., *Fluid Mechanics*, McGraw-Hill, Inc., 4th Ed., 1999.

THIS PAGE INTENTIONALLY LEFT BLANK

INITIAL DISTRIBUTION LIST

1. Defense Technical Information Center
   Ft. Belvoir, Virginia

2. Dudley Knox Library
   Naval Postgraduate School
   Monterey, California